

UNIVERSIDAD DE CONCEPCIÓN



CENTRO DE INVESTIGACIÓN EN
INGENIERÍA MATEMÁTICA (CI²MA)



A degenerating convection-diffusion system modelling froth
flotation with drainage

RAIMUND BÜRGER, STEFAN DIEHL,
MARÍA CARMEN MARTÍ, YOLANDA VÁSQUEZ

PREPRINT 2022-06

SERIE DE PRE-PUBLICACIONES

A degenerating convection-diffusion system modelling froth flotation with drainage

RAIMUND BÜRGER

*C²MA and Departamento de Ingeniería Matemática,
Universidad de Concepción, Casilla 160-C, Concepción, Chile*

STEFAN DIEHL

Centre for Mathematical Sciences, Lund University, P.O. Box 118, S-221 00 Lund, Sweden

M. CARMEN MARTÍ

*Departament de Matemàtiques, Universitat de València, Avda. Vicent Andrés Estellés s/n,
Burjassot, València, Spain*

YOLANDA VÁSQUEZ*

*C²MA and Departamento de Ingeniería Matemática,
Universidad de Concepción, Casilla 160-C, Concepción, Chile*

*Corresponding author: yvasquez@ing-mat.udec.cl

[Received on 9 February 2022]

Froth flotation is a common unit operation used in mineral processing. It serves to separate valuable mineral particles from worthless gangue particles in finely ground ores. The valuable mineral particles are hydrophobic and attach to bubbles of air injected into the pulp. This creates bubble-particle aggregates that rise to the top of the flotation column where they accumulate to a froth or foam layer that is removed through a launder for further processing. At the same time, the hydrophilic gangue particles settle and are removed continuously. The drainage of liquid due to capillarity is essential for the formation of a stable froth layer. This effect is included into a previously formulated hyperbolic system of partial differential equations that models the volume fractions of floating aggregates and settling hydrophilic solids [R. Bürger, S. Diehl and M.C. Martí, *IMA J. Appl. Math.* **84** (2019) 930–973]. The construction of desired steady-state solutions with a froth layer is detailed and feasibility conditions on the feed volume fractions and the volumetric flows of feed, underflow and wash water are visualized in so-called operating charts. A monotone numerical scheme is derived and employed to simulate the dynamic behaviour of a flotation column. It is also proven that, under a suitable Courant-Friedrichs-Lewy (CFL) condition, the approximate volume fractions are bounded between zero and one when the initial data are.

Keywords: froth flotation, sedimentation, drainage, capillarity, three-phase flow, conservation law, second-order degenerate parabolic PDE, steady states.

2000 Math Subject Classification: 35L65, 35P05, 35R05.

1. Introduction

1.1 Scope

Flotation is a separation process where air bubbles are used to attract hydrophobic particles or droplets from a mixture of solids in water. The process is used in mineral processing, where valuable mineral particles are separated out from crushed ore, and in wastewater treatment to remove floating solids,

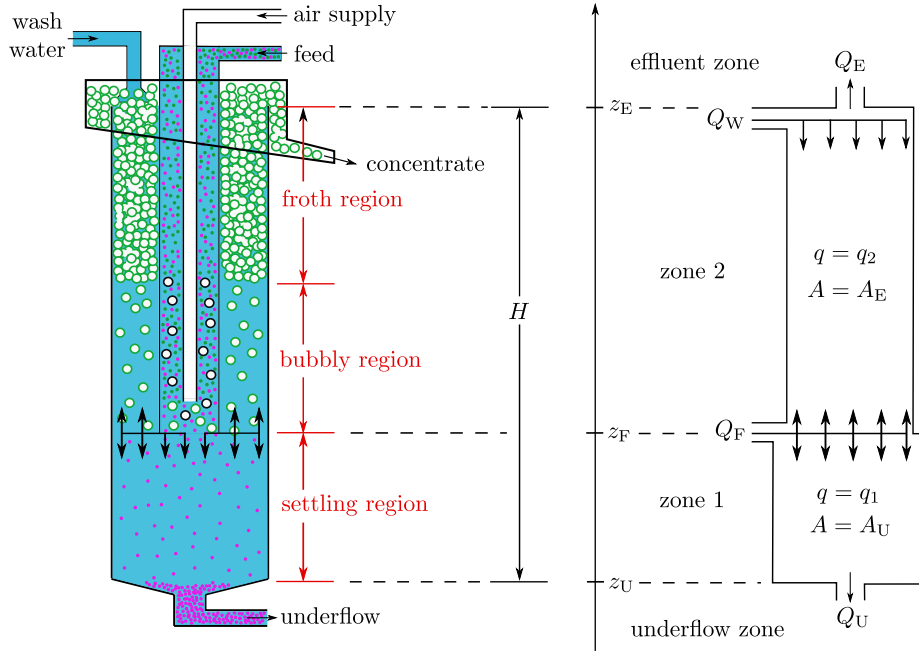


FIG. 1.1. Left: Schematic of a flotation column; cf. the Reflux Flotation Cell by Dickinson & Galvin (2014). Right: The corresponding one-dimensional conceptual model with a non-constant cross-sectional area $A(z)$. Wash water is sprinkled at the effluent level $z = z_E$ and a mixture of aggregates and feed slurry is fed at $z = z_F$, where $z_U < z_F < z_E$ divide the real line into the zones inside the column and the underflow and effluent zones.

residual chemicals, and droplets of oil and fat. The process is often applied in a column to which both a mixture of particles (or droplets) and air bubbles are injected. The effluent at the top should consist of a concentrate of hydrophobic particles that are attached to the bubbles, while the hydrophilic particles settle to the bottom, where they are removed (see Figure 1.1). A layer of froth at the top is preferred since the effluent then consists of a minimum amount of water and the froth works as a filter enhancing the separation process. In our previous models of column froth flotation (with or without simultaneous sedimentation of hydrophilic particles) (Bürger et al., 2018, 2019, 2020a,b), a particular constitutive assumption on the bubble velocity leads to a hyperbolic system of partial differential equations (PDEs) that models the layer of froth with a constant horizontal average volume fraction of bubbles ϕ , or equivalently, the volume fraction $\varepsilon = 1 - \phi$ of liquid (or suspension with hydrophilic particles) that fills the interstices outside the bubbles. It is however known that ε varies with the height in the froth because of capillarity and drainage of liquid; see Neethling & Brito-Parada (2018) and references therein.

It is the purpose of this work to extend the previous hyperbolic model to one that includes capillarity. To this end we partly generalize the well-known drainage equation to hold for all bubble volume fractions, and partly generalize our previous model of column froth flotation with simultaneous sedimentation. The latter is a nonlinear system of PDEs where the unknowns are the volume fractions of aggregates (bubbles/droplets loaded with hydrophobic particles) and solid hydrophilic particles. A numerical scheme for the new governing PDE system is presented. We show that the approximate volume fractions stay between zero and one if a suitable Courant-Friedrichs-Lewy (CFL) condition is used.

Furthermore, we construct desired steady-state solutions and provide algebraic equations and inequalities that establish the dependence of steady states on the input and control variables. Such dependences are conveniently visualized in so-called operating charts that constitute a graphical tool for controlling the process. The particular importance of steady states comes from the application under study; namely they describe the ability of the model to capture steady operation of the flotation device without the necessity of permanent control actions.

1.2 Some preliminaries

Froth is assumed to form when the volume fraction of bubbles ϕ is above a critical value $\phi_c = 1 - \varepsilon_c$ when the bubbles are in contact with each other. Then capillarity forces are involved, which means that the governing PDE is parabolic, whereas it is hyperbolic in regions without froth. The present derivation is based on the traditional one by Leonard & Lemlich (1965), Gol'dfarb et al. (1988), and Verbist et al. (1996), leading to the drainage equation for low liquid content ε . We then combine results by Neethling et al. (2002) and Stevenson & Stevanov (2004) to obtain a constitutive relationship between the relative fluid-gas velocity u and the liquid volume fraction $\varepsilon \leq \varepsilon_c$ when capillarity forces are present. With a compatibility condition at ε_c , we obtain a constitutive relationship of the relative fluid-bubble velocity u as a function of $\varepsilon \in [0, 1]$, which for $\varepsilon > \varepsilon_c$ is the common Richardson & Zaki (1954) power-law expression for separated bubbles (Galvin & Dickinson, 2014). The resulting generalized drainage PDE is (in a closed vessel)

$$\partial_t \varepsilon - \partial_z (\varepsilon \tilde{v}_f(\varepsilon)) = \partial_z^2 \tilde{D}(\varepsilon), \quad (1.1)$$

where t is time, z is height, $\tilde{v}_f(\varepsilon)$ is a nonlinear fluid-velocity function, and $\tilde{D}(\varepsilon)$ an integrated diffusion function modelling capillarity, which is zero for $\varepsilon > \varepsilon_c$.

Equation (1.1) can alternatively be written in terms of the volume fraction of bubbles ϕ . We assume that ϕ denotes the volume fraction of aggregates, by which we mean bubbles that are fully loaded with hydrophobic particles. Under a common constitutive assumption for the settling of hydrophilic particles within the liquid outside the bubbles, the following system of PDEs models the combined flotation-drainage-sedimentation process in a vertical column with a feed inlet of air-slurry mixture at the height $z = z_F$ with the volumetric flow $Q_F(t)$ (see Figure 1.1):

$$\begin{aligned} A(z) \partial_t \begin{pmatrix} \phi \\ \psi \end{pmatrix} + \partial_z \left(A(z) \begin{pmatrix} J(\phi, z, t) \\ -\tilde{F}(\psi, \phi, z, t) \end{pmatrix} \right) \\ = \partial_z \left(A(z) \gamma(z) \partial_z D(\phi) \begin{pmatrix} 1 \\ -\psi/(1-\phi) \end{pmatrix} \right) + Q_F(t) \begin{pmatrix} \phi_F(t) \\ \psi_F(t) \end{pmatrix} \delta_{z_F}. \end{aligned} \quad (1.2)$$

Here, ψ is the volume fraction of solids, $A(z)$ the cross-sectional area of the tank, and J and \tilde{F} are convective flux functions that depend discontinuously on z at the locations of the feed and wash water inlets and the outlets at the top and bottom. The system (1.2) is valid for $t > 0$ and all $z \in \mathbb{R}$ where the characteristic function $\gamma(z) = 1$ indicates the interior of the tank and $\gamma(z) = 0$ outside, and δ is the delta function. Outside the tank, the mixture is assumed to follow the outlet streams; consequently, boundary conditions are not needed; conservation of mass determines the outlet volume fractions in a natural way.

Similarly to the role of \tilde{D} in (1.1), the nonlinear function D models the capillarity present when bubbles are in contact. Precisely, with a function $d(\phi)$ (specified later) we define

$$D(\phi) := \int_0^\phi d(s) ds. \quad (1.3)$$

The function d is assumed to satisfy

$$d(\phi) = D'(\phi) = \begin{cases} 0 & \text{for } 0 \leq \phi \leq \phi_c, \\ > 0 & \text{for } \phi_c < \phi \leq 1. \end{cases} \quad (1.4)$$

Consequently, at each point (z, t) where $\phi(z, t) \leq \phi_c$, there holds $D(\phi(z, t)) = 0$, and therefore (1.2) degenerates at such points into a first-order system of conservation laws of hyperbolic type (as was shown in Bürger et al. (2019)). Since this degeneration occurs for $0 \leq \phi \leq \phi_c$ and $0 \leq \psi \leq 1 - \phi$, that is, on a set of positive two-dimensional measure, (1.2) is called *strongly degenerate*. While it is clear that the first PDE in (1.2) is parabolic for $\phi_c < \phi \leq 1$ and this PDE, as well as (1.1), are scalar strongly degenerate parabolic equations, the same cannot be said about the system. We observe namely that with $A = \gamma = 1$, the diffusion term on the right-hand side can be written as

$$\partial_z \left(d(\phi) \partial_z \phi \begin{pmatrix} 1 \\ -\psi/(1-\phi) \end{pmatrix} \right) = \partial_z \left(\mathbf{B}(\phi, \psi) \begin{pmatrix} \partial_z \phi \\ \partial_z \psi \end{pmatrix} \right), \quad \mathbf{B}(\phi, \psi) := d(\phi) \begin{bmatrix} 1 & 0 \\ -\psi/(1-\phi) & 0 \end{bmatrix}.$$

Since at least one of the eigenvalues of $\mathbf{B}(\phi, \psi)$ is always zero, we observe that even when $d(\phi) > 0$, the system (1.2) is not *strictly* parabolic.

1.3 Related work

Modelling flotation and developing strategies to control this process are research areas that have generated many contributions; see Cruz (1997) and the review by Quintanilla et al. (2021) and references therein. The development of control strategies requires dynamic models along with a categorization of steady-state (stationary) solutions of such models. Since the volume fractions depend on both time and space, the resulting governing equations are PDEs. With the aim of developing controllers, Tian et al. (2018a,b) and Azhin et al. (2021a,b) use hyperbolic systems of PDEs for the froth or pulp regions coupled to ODEs for the lower part of the column. They include the attachment and detachment processes; however, the phases seem to have constant velocities, which is not in agreement with the established drift-flux theory (Wallis, 1969; Rietema, 1982; Brennen, 2005). Nonlinear dependence of the phase velocities on the volume fractions give rise to discontinuities in the concentration profiles, which is confirmed experimentally (Cruz, 1997). Azhin et al. (2021a,b) show continuous steady-state profiles for their model.

Narsimhan (2010) shows realistic conceptual transient solutions of a bubble-liquid suspension which is homogeneous initially. The rising bubbles form a layer of foam at the top which can undergo compressibility due to gravity and capillarity. The governing PDE has similarities with (1.1); however, it is not utilized in all the different regions of solution. Separate equations are derived for the foam region and boundary assumptions between regions have to be imposed. The purpose of our previous and the present contributions is to let a single equation such as (1.1) govern the bubble-liquid behaviour under any dynamic situation.

Phenomenological models for two-phase systems with bubbles rising (or, analogously, particles settling) in a liquid, are derived from physical laws of conservation of mass and momentum (Bascur, 1991; Bustos et al., 1999; Bürger et al., 2000; Brennen, 2005). Under certain simplifying assumptions on the stress tensor and partial pressure of the bubbles/solids, one can obtain first- or second-order PDEs involving one or two constitutive (material specific) functions, respectively.

The resulting first-order PDE modelling such a separation process in a one-dimensional column of rising bubbles is a scalar conservation law $\phi_t + (\phi \tilde{v}(\phi))_z = 0$ with a drift-flux velocity function $\tilde{v}(\phi)$.

This is in agreement with the drift-flux theory by Wallis (1969). With additional bulk flows due to the inlets and outlets of the column that theory has mostly been used for steady-state investigations of flotation columns (Vandenberghe et al., 2005; Stevenson et al., 2008; Dickinson & Galvin, 2014; Galvin & Dickinson, 2014; Galvin et al., 2014). Models of and numerical schemes for column froth flotation with the drift-flux assumption and possibly simultaneous sedimentation have been presented by the authors (Bürger et al., 2018, 2019, 2020a,b).

The analogy of the drift-flux theory for sedimentation is the established solids-flux theory (Kynch, 1952; Ekama et al., 1997; Diehl, 2001, 2008b; Ekama & Marais, 2004; La Motta et al., 2007). With an additional constitutive assumption on sediment compressibility, the model becomes a second-order degenerate parabolic PDE (Bürger et al., 2000). Sedimentation in a clarifier-thickener unit is mathematically similar to the column-flotation case. A full PDE model of such a vessel necessarily contains source terms and spatial discontinuities at both inlets and outlets. Steady-state analyses, numerical schemes, dynamic simulations and control of such models can be found in Bürger et al. (2004, 2005) and Diehl (1996, 1997, 2008a). Because of the discontinuous coefficients and degenerate diffusion term of the PDE, so-called entropy conditions are needed to guarantee a unique physically relevant solution (Bürger et al., 2005; Evje & Karlsen, 2000; Diehl, 2009). Those results will be utilized in the present work.

The first-order PDE of the flotation process does not include capillarity in the foam. Such effects have been studied intensively by Neethling and Cilliers (Neethling et al., 2002; Neethling & Cilliers, 2003) and Neethling and Brito-Parada (Neethling & Brito-Parada, 2018); see more references in Quintanilla et al. (2021). Solids motion in froth can be found in Neethling & Cilliers (2002). It is the aim of the present contribution to extend our previous hyperbolic PDE model to include capillarity.

1.4 Outline of the paper

In Section 2, we consider a simplified two-phase bubble-fluid system in a closed vessel and derive a generalized drainage equation governing the flotation of the bubbles with formation of froth and drainage of liquid from it. In Section 3, we extend the equation derived to the process of column flotation with sedimentation of solid particles and with froth drainage at the top. The treatment of the feed inlets and the definition of the flux density functions in each zone (see Figure 1.1) are detailed. Section 4 is devoted to the construction of steady-state solutions having a froth layer at the top of the tank and bubble-free underflow. Necessary conditions for those so-called desired steady-states to appear, in terms of inequalities involving the volumetric flows Q_U , Q_F and Q_W and the incoming volume fractions of aggregates ϕ_F and solids ψ_F , are derived in Sections 4.4 and 4.5. In Section 5, the numerical scheme for simulation of the process is introduced. It is proven that under a CFL condition, the approximate volume fractions of aggregates and solids remain between zero and one provided that the initial data do. The proofs are outlined in Appendix A. Some simulations are provided in Section 6. They show fill-up of a flotation column and froth formation, illustrating the response of the system to changes of operating conditions. Finally, conclusions are drawn in Section 7.

2. A generalized drainage equation in a closed tank

The two-phase system has bubbles of volume fraction ϕ and phase velocity v , and fluid of volume fraction $\varepsilon = 1 - \phi$ and phase velocity v_f , where $0 \leq \phi, \varepsilon \leq 1$. When the bubbles are mono-sized and separated from each other (i.e., there is no froth), a common expression for their velocity in a closed container without any bulk flow is (Pal & Masliyah, 1989; Vandenberghe et al., 2005)

$$v(\phi) = v_{\text{term}}(1 - \phi)^{n_b} \quad (\text{separated bubbles}),$$

where v_{term} is the velocity of a single bubble far away from others ($\phi \approx 0$) and n_b a dimensionless parameter (similar to the Richardson-Zaki exponent within the analogous expression for the sedimentation of mono-sized and equal-density particles in a liquid, see Section 3.3). We thus let velocities be positive in the upward direction of the z -axis. The relative velocity of fluid to bubbles is $u := v_f - v$. In a closed container, the volume-average velocity is zero; hence, $0 = \phi v + \varepsilon v_f$, and we get

$$u = -\frac{(1-\varepsilon)v}{\varepsilon} - v = -\frac{v}{\varepsilon} = -v_{\text{term}}\varepsilon^{n_b-1} \quad (\text{separated bubbles}), \quad (2.1)$$

which is negative because the fluid flows downwards. We also obtain the identities $v_f = (1-\varepsilon)u$ and $v = -(1-\phi)u$.

If ϕ exceeds a certain critical volume fraction $\phi_c = 1 - \varepsilon_c$, the bubbles touch each other and a foam is formed. The larger $\phi > \phi_c$, or smaller $\varepsilon < \varepsilon_c$, the more deformed are the bubbles. Randomly packed rigid spheres leave a volume fraction of $\varepsilon_c = 1 - 0.64 = 0.36$; cf. (Brito-Parada et al., 2012, Table 1). For froth, we assume the value $\varepsilon_c = 0.26$ (Neethling & Cilliers, 2003, Eq. (21)) and Narsimhan (2010).

We discuss below the most difficult intermediate fluid volume fractions when ε is smaller than, but close to ε_c . We consider, however, first a layer of foam with a very low volume fraction of liquid ε and recall the derivation of the drainage equation (Leonard & Lemlich, 1965; Gol'dfarb et al., 1988; Verbist et al., 1996). In this case the deformed bubbles are separated by very thin lamellae, which are separated by channels, so called *Plateau borders*, which are connected at vertices, or nodes, so that a network is formed. It is assumed that almost all the liquid is contained in the Plateau borders, whose cross section is the plane region bounded by three externally tangential circles all of radius r . This deformed triangular-shaped region has the area

$$\mathcal{A} = C^2 r^2, \quad \text{with } C := (\sqrt{3} - \pi/2)^{1/2}. \quad (2.2)$$

If the radius r changes along the Plateau border, this is related to a pressure difference according to the Young-Laplace law:

$$p_f = p_b - \frac{\gamma_w}{r},$$

where p_f and p_b are the fluid and bubble pressure, respectively, and γ_w is the surface tension of water. The bubble pressure p_b is assumed to be constant.

There are three forces acting per volume fraction of the Plateau border:

$$\begin{aligned} \text{gravity:} & \quad \rho_f \mathbf{g}, \\ \text{dissipation:} & \quad -\frac{C_{\text{PB}} \mu}{\mathcal{A}} \mathbf{u} = -\frac{C_{\text{PB}} \mu}{C^2 r^2} \mathbf{u}, \\ \text{capillarity:} & \quad -\nabla p_f = -\frac{\gamma_w}{r^2} \nabla r. \end{aligned}$$

Here, \mathbf{g} is the gravity acceleration vector, \mathbf{u} the fluid-bubble relative velocity, μ the fluid viscosity, and C_{PB} the dimensionless Plateau border drag coefficient, which can be inferred to be 49.3 from the numerical calculations by Leonard & Lemlich (1965). The value $C_{\text{PB}} = 50$ is often used in the literature. The sum of the three forces is zero if one neglects inertial forces. Along a Plateau border tilted an angle θ from the vertical z -axis, we place a z_θ -axis with the coordinate relation $z = z_\theta \cos \theta$. The force balance along the z_θ -axis is

$$-\rho_f g \cos \theta - \frac{C_{\text{PB}} \mu}{C^2 r^2} u_\theta - \frac{\gamma_w}{r^2} \partial_{z_\theta} r = 0,$$

where the relative fluid-gas velocity in the channel is $u_\theta = u_{\text{PB}}/\cos\theta$ and u_{PB} is its vertical contribution from one Plateau border of angle θ , which thus is

$$u_{\text{PB}} = -\frac{C^2 r^2}{C_{\text{PB}} \mu} \left(\rho_{\text{fg}} + \frac{\gamma_{\text{w}}}{r^2} \partial_z r \right) \cos^2 \theta.$$

Under the assumption of randomly distributed Plateau borders with respect to the angle $0 \leq \theta \leq \pi$, the likelihood that a Plateau border has an angle in the interval $(\theta, \theta + d\theta)$ is the area $2\pi \sin\theta d\theta$ of the circular strip of the unit sphere divided by its total area 4π . Since

$$\langle \cos^2 \rangle := \int_0^\pi \cos^2 \theta \frac{2\pi \sin \theta}{4\pi} d\theta = \frac{1}{3},$$

the relative vertical velocity u is defined as the average vertical relative fluid-gas velocity for many Plateau borders:

$$u = \langle u_{\text{PB}} \rangle = -\frac{C^2 r^2 \rho_{\text{fg}}}{3 C_{\text{PB}} \mu} \left(1 + \frac{\gamma_{\text{w}}}{r^2 \rho_{\text{fg}}} \partial_z r \right). \quad (2.3)$$

This velocity can be expressed in \mathcal{A} by (2.2), and substituting the resulting expression into the conservation law $\partial_t \mathcal{A} + \partial_z (\mathcal{A}(1-\varepsilon)u) = 0$ and setting $\varepsilon = 0$ (recall that $v_{\text{f}} = (1-\varepsilon)u$) one obtains the classical drainage equation for low liquid content.

We want an equation for the volume fraction ε , which is equal to \mathcal{A} times the length of Plateau borders per unit volume; cf. Neethling & Brito-Parada (2018). Then the length L and number of such channels should be estimated. Since we also want an equation for all $0 \leq \varepsilon \leq \varepsilon_{\text{c}}$, the estimation of such numbers becomes difficult since the Plateau borders are only narrow channels for small ε , their lengths are not well defined and the volume and dissipation effect in the nodes varies. Koehler et al. (2000) presented a relationship between ε , L and r , valid for at least ε up to 0.1. They derived a generalized foam drainage equation which covers the two limiting cases of channel- and node-dominated models, respectively. To remove the variable L , Neethling et al. (2002) made the common assumption that for small ε , bubbles can be assumed to have the form of a tetrakaidecahedron (Kelvin cell) and used the equation $4\pi r_{\text{b}}^3/3 = (1-\varepsilon)2^{2/7}L^3$, where r_{b} is the bubble radius. Thereby, they obtained the algebraic equation

$$\varepsilon = 0.3316 \left(\frac{r}{r_{\text{b}}} \right)^2 (1-\varepsilon)^{2/3} + 0.5402 \left(\frac{r}{r_{\text{b}}} \right)^3 (1-\varepsilon), \quad (2.4)$$

which is implicit in all its variables. Containing these three variables, they derived a PDE valid for $0 \leq \varepsilon \leq \varepsilon_{\text{c}}$ by considering dissipation both from the Plateau borders and the nodes. Assuming r_{b} is constant, their PDE and algebraic equation defines the unknowns ε and r .

Stevenson (2006) demonstrated that the effective relative fluid-gas velocity u could be very well approximated by a power law of the type (2.1), at least for fluid volume fraction up to $\varepsilon \approx 0.2$. In particular, Stevenson & Stevanov (2004) approximated Equation (2.4) by

$$\frac{r}{r_{\text{b}}} = m \varepsilon^{n_{\text{S}}}, \quad \text{with } m = 1.28, n_{\text{S}} = 0.46.$$

This equation can be substituted into (2.3) to give

$$u = -v_{\text{drain}} \varepsilon^{2n_{\text{S}}} (1 + d_{\text{cap}} \varepsilon^{-(1+n_{\text{S}})} \partial_z \varepsilon) \quad \text{for } 0 \leq \varepsilon < \varepsilon_{\text{c}}, \quad (2.5)$$

where the drainage velocity v_{drain} (with respect to gravity and dissipation) and the dimensionless capillarity-to-gravity parameter d_{cap} are given by

$$v_{\text{drain}} := \frac{m^2 C^2 r_b^2 \rho_f g}{3 C_{\text{PB}} \mu}, \quad d_{\text{cap}} := \frac{n_S \gamma_w}{m r_b \rho_f g}.$$

The derivative term in (2.5) models the capillarity that is not present for separated bubbles; see (2.1). Hence, we suggest the relative fluid-gas velocity

$$u := - \begin{cases} v_{\text{drain}} \varepsilon^{2n_S} (1 + d_{\text{cap}} \varepsilon^{-(1+n_S)} \partial_z \varepsilon) & \text{for } 0 \leq \varepsilon < \varepsilon_c, \\ v_{\text{term}} \varepsilon^{n_b-1} & \text{for } \varepsilon_c \leq \varepsilon \leq 1 \end{cases}$$

with the compatibility condition (continuity across $\varepsilon = \varepsilon_c$)

$$v_{\text{drain}} \varepsilon_c^{2n_S} = v_{\text{term}} \varepsilon_c^{n_b-1} \quad \Leftrightarrow \quad \frac{v_{\text{drain}}}{v_{\text{term}}} = \varepsilon_c^{n-1-2n_S}. \quad (2.6)$$

Values for n_b in the literature range from 2 to 3.2 (Dickinson & Galvin, 2014; Galvin & Dickinson, 2014; Pal & Masliyah, 1989; Vandenberghe et al., 2005).

Recalling once again that $v_f = (1 - \varepsilon)u$, we now define the velocity function

$$\tilde{v}_f(\varepsilon) := \begin{cases} v_{\text{drain}} (1 - \varepsilon) \varepsilon^{2n_S} & \text{for } 0 \leq \varepsilon < \varepsilon_c, \\ v_{\text{term}} (1 - \varepsilon) \varepsilon^{n_b-1} & \text{for } \varepsilon_c \leq \varepsilon \leq 1 \end{cases}$$

and the diffusion function

$$d_f(\varepsilon) := \begin{cases} v_{\text{drain}} d_{\text{cap}} (1 - \varepsilon) \varepsilon^{n_S} & \text{for } 0 \leq \varepsilon < \varepsilon_c, \\ 0 & \text{for } \varepsilon_c \leq \varepsilon \leq 1, \end{cases}$$

so that the liquid flux (in a closed vessel) becomes

$$\varepsilon v_f = \varepsilon (1 - \varepsilon) u = -\varepsilon \tilde{v}_f(\varepsilon) - d_f(\varepsilon) \partial_z \varepsilon = -\varepsilon \tilde{v}_f(\varepsilon) - \partial_z \tilde{D}(\varepsilon), \quad (2.7)$$

where the integrated diffusion function is

$$\tilde{D}(\varepsilon) := \int_0^\varepsilon d_f(\xi) d\xi = \begin{cases} v_{\text{drain}} d_{\text{cap}} \left(\frac{\varepsilon^{n_S+1}}{n_S+1} - \frac{\varepsilon^{n_S+2}}{n_S+2} \right) & \text{for } 0 \leq \varepsilon < \varepsilon_c, \\ v_{\text{drain}} d_{\text{cap}} \left(\frac{\varepsilon_c^{n_S+1}}{n_S+1} - \frac{\varepsilon_c^{n_S+2}}{n_S+2} \right) & \text{for } \varepsilon_c \leq \varepsilon \leq 1. \end{cases}$$

(Notice that $\tilde{D}(\varepsilon)$ is constant, and therefore $\tilde{D}'(\varepsilon) = 0$, for $\varepsilon_c \leq \varepsilon \leq 1$.) Inserting the expression (2.7) into the conservation law for the fluid phase $\partial_t \varepsilon + \partial_z(\varepsilon v_f) = 0$, we obtain the generalized Equation (1.1) modelling both rising bubbles and drainage of froth in a closed container.

3. A model of flotation including froth drainage

3.1 Assumption on the tank and mixture

We use a one-dimensional setup of the Reflux Flotation Cell by Dickinson & Galvin (2014); see Figure 1.1. A mixture of slurry and aggregates is fed at the height $z = z_F$ at the volumetric flow $Q_F > 0$ and

wash water is injected at the top effluent level $z = z_E$ at $Q_W \geq 0$. At $z = z_U$, a volumetric flow $Q_U \geq 0$ is taken out. In the one-dimensional model on the real line, there are four zones, two inside the vessel plus the underflow and effluent zones. The resulting effluent volumetric overflow $Q_E := Q_W + Q_F - Q_U$ is assumed to be positive so that the mixture is conserved and the vessel is always completely filled. In comparison to the previous treatments (Bürger et al., 2019, 2020a), here we do not separate the wash water inlet and the effluent level, i.e., $z_W = z_E$. The cross-sectional area is assumed to satisfy

$$A(z) = \begin{cases} A_E & \text{for } z \geq z_F, \\ A_U & \text{for } z < z_F. \end{cases}$$

Particles trapped in the froth region influence the drainage of fluid (Ata, 2012; Haffner et al., 2015), but for simplicity we nevertheless assume that the volume fraction of aggregates (bubbles with attached hydrophobic particles) can be determined as a function of height and time by a single equation. Thus, the suspension in the interstices outside the bubbles is assumed to behave independently of the volume fraction of (hydrophilic) particles. Such particles may however settle within the suspension, which undergoes bulk transport. From now on we denote by $\phi = 1 - \varepsilon$ the volume fraction of aggregates. As a first approximation in a closed vessel, ϕ can be obtained by solving (1.1) for ε and setting $\phi = 1 - \varepsilon$, but we proceed to derive an explicit equation for ϕ since that will be extended to the more complicated model of a flotation column with in- and outlets.

3.2 Equation for aggregates with froth drainage in a closed tank

We recall the gas-phase velocity $v = -(1 - \phi)u$ and the compatibility condition (2.6), and define

$$\tilde{v}(\phi) := \begin{cases} v_{\text{term}}(1 - \phi)^{n_b} & \text{for } 0 \leq \phi \leq \phi_c, \\ v_{\text{drain}}(1 - \phi)^{2n_S+1} = v_{\text{term}} \frac{(1 - \phi)^{2n_S+1}}{(1 - \phi_c)^{2n_S+1-n_b}} & \text{for } \phi_c < \phi \leq 1, \end{cases} \quad (3.1)$$

$$d(\phi) := \begin{cases} 0 & \text{for } 0 \leq \phi \leq \phi_c, \\ v_{\text{drain}} d_{\text{cap}} \phi (1 - \phi)^{n_S} = v_{\text{term}} d_{\text{cap}} \frac{\phi (1 - \phi)^{n_S}}{(1 - \phi_c)^{2n_S+1-n_b}} & \text{for } \phi_c < \phi \leq 1. \end{cases} \quad (3.2)$$

With the batch-drift flux function $j_b(\phi) := \phi \tilde{v}(\phi)$, where $\tilde{v}(\phi)$ is given by (3.1), we can write the aggregate-phase flux (in a closed container) as

$$\phi v = -\phi(1 - \phi)u = \phi \tilde{v}(\phi) + d(\phi) \partial_z(1 - \phi) = \phi \tilde{v}(\phi) - d(\phi) \partial_z \phi = j_b(\phi) - \partial_z D(\phi),$$

where $D(\phi)$ is defined by (1.3). In light of (3.2) we obtain

$$D(\phi) = \begin{cases} 0 & \text{for } 0 \leq \phi \leq \phi_c, \\ v_{\text{drain}} d_{\text{cap}} \frac{\omega(\phi_c) - \omega(\phi)}{(n_S + 1)(n_S + 2)} & \text{for } \phi_c < \phi \leq 1, \end{cases} \quad (3.3)$$

where $\omega(\phi) := (1 - \phi)^{n_S+1}((n_S + 1)\phi + 1)$ and we reconfirm the property (1.4). The conservation law $\partial_t \phi + \partial_z(\phi v) = 0$ now yields the following equation for the volume fraction $\phi = \phi(z, t) \in [0, 1]$ of aggregates in a closed vessel:

$$\partial_t \phi + \partial_z j_b(\phi) = \partial_z^2 D(\phi). \quad (3.4)$$

The graphs of the constitutive functions $j_b(\phi)$ and $D(\phi)$ are drawn in Figure 3.1.

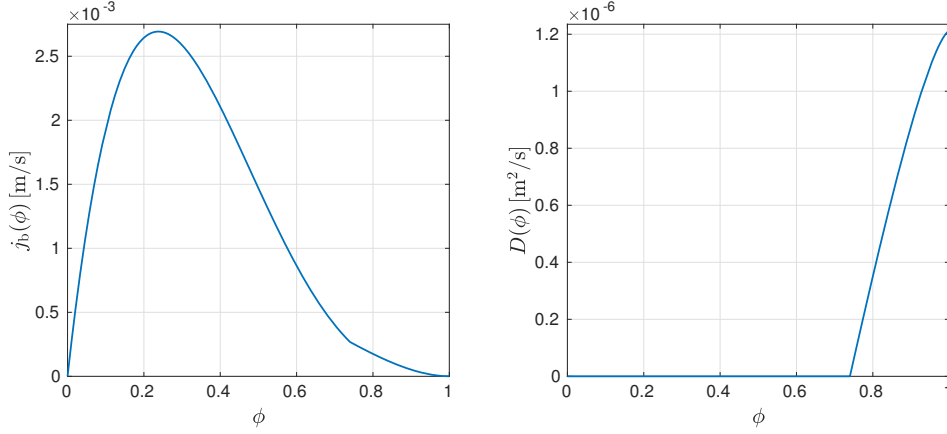


FIG. 3.1. Left: function $j_b(\phi) = \phi \tilde{v}(\phi)$. Right: diffusion function $D(\phi)$ modelling capillarity. Note the behaviour of these functions at the critical concentration $\phi_c = 0.74$.

3.3 Three phases and constitutive assumptions

The three phases and their volume fractions are the fluid ϕ_f , the solids ψ , and the aggregates ϕ , where $\phi_f + \psi + \phi = 1$. By suspension we mean the fluid and solid phases. The volume fraction of solids *within the suspension* φ is defined by

$$\varphi := \frac{\psi}{\psi + \phi_f} = \frac{\psi}{1 - \phi}.$$

The drift-flux and solids-flux theories utilize constitutive functions for the aggregate upward batch flux $j_b(\phi)$ and the solids batch sedimentation flux $f_b(\varphi) := \varphi v_{\text{hs}}(\varphi)$, where $v_{\text{hs}}(\varphi)$ is the hindered-settling function. For simplicity, we employ the common expression (Richardson & Zaki, 1954)

$$v_{\text{hs}}(\varphi) = v_\infty (1 - \varphi)^{n_{\text{RZ}}}, \quad \text{where } n_{\text{RZ}} > 1. \quad (3.5)$$

Applying the conservation of mass to each of the three phases, introducing the volume-average velocity, or bulk velocity, of the mixture q and the relative velocities of both the aggregate-suspension and the solid-fluid, Bürger et al. (2019) derived the PDE model (1.2) without the capillarity function $D(\phi)$. In particular, the volumetric flows in and out of the flotation column define explicitly

$$q(z, t) := \begin{cases} q_E := (-Q_U + Q_F + Q_W)/A_E & \text{for } z \geq z_E, \\ q_2 := (-Q_U + Q_F)/A_E & \text{for } z_F \leq z < z_E, \\ q_1 = q_U := -Q_U/A_U & \text{for } z < z_F. \end{cases} \quad (3.6)$$

In the underflow and effluent zones all phases are assumed to have the same velocity, i.e., they follow the bulk flow. Then the total convective fluxes for ϕ and φ are given by

$$J(\phi, z, t) = \begin{cases} j_E(\phi, t) := q_E(t)\phi & \text{for } z \geq z_E, \\ j_2(\phi, t) := q_2(t)\phi + j_b(\phi) & \text{for } z_F \leq z < z_E, \\ j_1(\phi, t) := q_1(t)\phi + j_b(\phi) & \text{for } z_U \leq z < z_F, \\ j_U(\phi, t) := q_1(t)\phi & \text{for } z < z_U, \end{cases}$$

$$F(\varphi, \phi, z, t) = \begin{cases} f_E(\varphi, \phi, t) := -(1-\phi)q_E(t)\varphi & \text{for } z \geq z_E, \\ f_2(\varphi, \phi, t) & \text{for } z_F \leq z < z_E, \\ f_1(\varphi, \phi, t) & \text{for } z_U \leq z < z_F, \\ f_U(\varphi, \phi, t) := -(1-\phi)q_1(t)\varphi & \text{for } z < z_U \end{cases}$$

with the zone-settling flux functions (positive in the direction of sedimentation (decreasing z))

$$\begin{aligned} f_k(\varphi, \phi, t) &:= (1-\phi)f_b(\varphi) + (j_b(\phi) - (1-\phi)q_k(t))\varphi \\ &= (1-\phi)f_b(\varphi) + (j_k(\phi, t) - q_k(t))\varphi, \quad k = 1, 2. \end{aligned}$$

With the capillarity function $D(\phi)$, the batch flux $j_b(\phi)$ is extended to $j_b(\phi) - \partial_z D(\phi)$; cf. (3.4). Hence, the total flux of the aggregates for any $z \in \mathbb{R}$ is

$$\Phi(\phi, \partial_z \phi, z, t) := J(\phi, z, t) - \gamma(z)\partial_z D(\phi),$$

where the characteristic function is

$$\gamma(z) := \begin{cases} 1 & \text{for } z \in [z_U, z_E), \\ 0 & \text{for } z \notin [z_U, z_E), \end{cases}$$

and the total flux of the solids in the z -direction is (F and \tilde{F} are positive in the downwards direction of sedimentation, which is opposite to the z -direction)

$$\Psi(\psi, \partial_z \psi, \phi, z, t) := -\tilde{F}(\psi, \phi, z, t) + \gamma(z)\frac{\Psi}{1-\phi}\partial_z D(\phi), \quad (3.7)$$

where

$$\tilde{F}(\psi, \phi, z, t) := \begin{cases} F\left(\frac{\Psi}{1-\phi}, \phi, z, t\right) & \text{if } 0 \leq \phi < 1, \\ 0 & \text{if } \phi = 1. \end{cases}$$

The conservation law applied on the two phases with the total fluxes Φ and Ψ yields the governing system of equations (1.2) in the case capillarity are included. That system defines solutions on the real line and next we define the outlet concentrations of the flotation column.

3.4 Outlet concentrations

Given the PDE solutions $\phi = \phi(z, t)$ and $\varphi = \varphi(z, t)$ of (1.2), we define the boundary concentrations at each in- or outlet by $\phi_U^\pm = \phi_U^\pm(t) := \phi(z_U^\pm, t)$, etc. Conservation of mass across $z = z_U$ yields

$$j_1(\phi_U^+, t) - \partial_z D(\phi)|_{z=z_U^+} = j_U(\phi_U^-, t), \quad (3.8)$$

$$f_1(\varphi_U^+, t) - \varphi_U^+ \partial_z D(\phi)|_{z=z_U^+} = f_U(\varphi_U^-, t). \quad (3.9)$$

The underflow concentrations of the flotation column are defined by $\phi_U(t) := \phi_U^-(t)$ and $\varphi_U(t) := \varphi_U^-(t)$. These concentrations can in fact be obtained from the solution inside the column ($z_U < z < z_E$) from (3.8) and (3.9) together with a uniqueness condition; see Diehl (2009).

For the effluent level $z = z_E$, the analogous situation holds:

$$j_2(\phi_E^-, t) - \partial_z D(\phi)|_{z=z_E^-} = j_E(\phi_E^+, t), \quad (3.10)$$

$$f_2(\varphi_E^-, \phi_E^-, t) - \varphi_E^- \partial_z D(\phi)|_{z=z_E^-} = f_E(\varphi_E^+, \phi_E^+, t), \quad (3.11)$$

In the one-dimensional PDE model (1.2) without boundary conditions, the solution $\phi = \phi(z, t)$ (analogously for φ) in the interval $z > z_E$ is governed by the linear transport PDE $\partial_t \phi + (Q_E/A_E) \partial_z \phi = 0$ and the boundary value $\phi_E^+(t)$. The effluent outlet concentrations are defined by $\phi_E := \phi_E^+$ and $\varphi_E := \varphi_E^+$. In the concluding section, we discuss how bursting bubbles at the top can be incorporated in the model.

4. Steady-state analysis

4.1 Definition of a desired steady state

In the case of no capillarity, Bürger et al. (2019) provided detailed constructions of all steady states, and Bürger et al. (2020a,b) sorted out the most interesting steady states for the applications and how to control these by letting the volumetric flows satisfy certain nonlinear inequalities, which can be visualized in so-called operating charts. We assume that Q_F , ϕ_F , and ψ_F are given variables and that Q_U and Q_W are control variables. The purpose here is to provide an improved model of the froth region and we therefore focus on the steady states when a layer of froth in zone 2 is possible. We consider only solutions where the froth layer does not fill the entire zone 2, so that there is at least a small region above the feed inlet with aggregate volume fraction below the critical one. As mentioned before, it is assumed that the wash water is sprinkled at the top of the column, which is commonly done and gives fewer steady states to analyse. A *desired steady state* is defined to be a stationary solution that has

$$\begin{aligned} \text{no aggregates below the feed level} &\Rightarrow \phi_U = 0, \\ \text{no solids above the feed level} &\Rightarrow \phi_E = 0, \\ \text{a froth layer that does not fill the entire zone 2} &\Rightarrow \phi(z_F^+) < \phi_c. \end{aligned} \quad (4.1)$$

The reversed implications do not hold in the two first statements for the following reasons. Since the bulk flow in zone 1 is directed downwards, there exist steady-state solutions with a standing layer of aggregates below the feed level. Analogously, if the bulk flow in zone 2 is directed upwards, there may be a layer of standing solids when their settling velocity is balanced by the upward bulk velocity; see Bürger et al. (2019).

4.2 Properties of the batch-flux density functions

With \tilde{v} given by (3.1), the continuous batch-drift flux function is

$$j_b(\phi) := \phi \tilde{v}(\phi) = \begin{cases} j_{bl}(\phi) := \phi v_{\text{term}} (1 - \phi)^{n_b} & \text{for } 0 \leq \phi \leq \phi_c, \\ j_{bh}(\phi) := \phi v_{\text{term}} \frac{(1 - \phi)^{2n_S + 1}}{(1 - \phi_c)^{2n_S + 1 - n_b}} & \text{for } \phi_c < \phi \leq 1, \end{cases}$$

where we have introduced the low j_{bl} and high j_{bh} parts of it. Any function $u \mapsto u(1 - u)^n$ has a unique inflection point at $u_{\text{infl}} = 2/(n + 1)$. Figure 4.1 shows the inflection points

$$\phi_{\text{infl},l}(n_b) = \frac{2}{n_b + 1}, \quad \phi_{\text{infl},h}(n_S) = \frac{2}{2n_S + 1 + 1} = \frac{1}{n_S + 1}$$

of j_{bl} and j_{bh} , as functions of the exponents n and n_S , respectively. With the values $\phi_c = 0.74$ and $n_S = 0.46$ suggested in the literature (see Section 2), and the interval $2 \leq n_b \leq 3.2$, there is only one

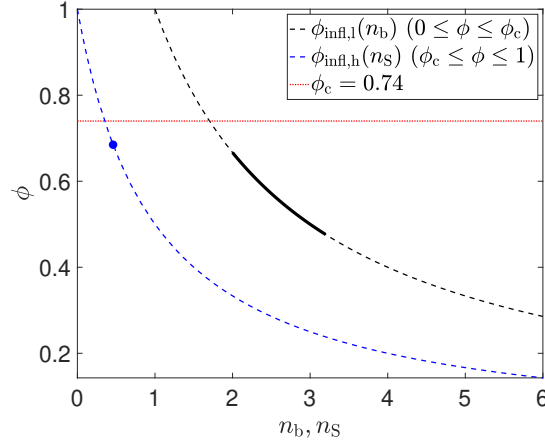


FIG. 4.1. Evolution of the inflection points of j_b and j_{bh} . The literature values $2 \leq n_b \leq 3.2$ give an interval (solid black) of possible $\phi_{\text{infl},l}$ that lie entirely below $\phi_c = 0.74$ (red line). With $n_S = 0.46$, the inflection point (blue dot) $\phi_{\text{infl},h} = 1/(n_S + 1) \approx 0.685 < \phi_c$; hence, j_{bh} is strictly convex for $\phi \geq \phi_c$.

inflection point of j_b in $0 \leq \phi \leq 1$ and this lies below ϕ_c ; see Figure 4.2, which also shows that there may be a jump in the derivative of j_b at $\phi = \phi_c$. Since

$$j'_b(\phi) = \begin{cases} v_{\text{term}}(1-\phi)^{n_b-1}(1-(1+n_b)\phi) & \text{for } 0 < \phi < \phi_c, \\ v_{\text{term}} \frac{(1-\phi)^{2n_S}(1-(2+2n_S)\phi)}{(1-\phi_c)^{2n_S+1-n_b}} & \text{for } \phi_c < \phi < 1, \end{cases}$$

we get that

$$j'_b(\phi_c^-) \leq j'_b(\phi_c^+) \Leftrightarrow n_b \geq 1 + 2n_S \approx 1.92. \quad (4.2)$$

When this is satisfied, the exponent in the compatibility condition (2.6) is nonnegative and the entire j_b has only one inflection point $\phi_{\text{infl}} = \phi_{\text{infl},l} \in (0, \phi_c)$.

4.3 Properties of the zone flux functions

The zone flux functions $j_k, f_k(\cdot, \phi)$, $k = 1, 2$, have an additional linear term due to the bulk velocity of the zone. Let $j(\phi) = j_b(\phi) + q\phi$ denote a general zone flux function, where we drop the t -variable when considering steady states. We will sometimes write out the dependence on q ; $j(\phi; q)$. The inflection point ϕ_{infl} of j is independent of q , however, the local maximum $\phi^M = \phi^M(q) < \phi_c$ depends on q . To provide an explicit definition, we first define

$$q_{\text{neg}} := -j'_b(0), \quad \bar{q} := -j'_b(\phi_{\text{infl}}).$$

For $q \leq q_{\text{neg}}$, $j(\cdot, q)$ is decreasing and for $q \geq \bar{q}$, $j(\cdot, q)$ is increasing. For intermediate values of q , the local maximum exists and satisfies $0 = j'(\phi^M) = j'_b(\phi^M) + q$. Since the restriction $(j_b|_{(0, \phi_{\text{infl}})})'$ is a

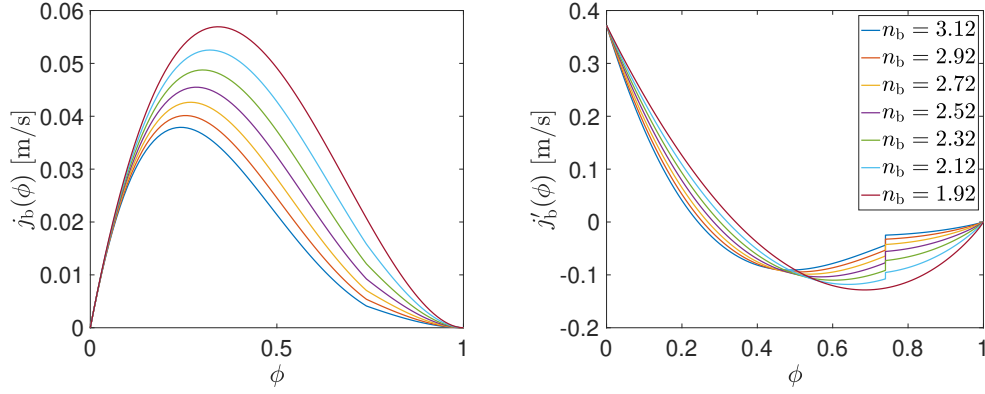


FIG. 4.2. Plots of $j_b(\phi)$ (left) and $j'_b(\phi)$ (right) for $n_S = 0.46$, $v_{\text{term}} = 0.3718$ and various values of n_b that satisfy (4.2).

strictly decreasing function, we can define

$$\phi^M = \phi^M(q) := \begin{cases} 0 & \text{if } q \leq q_{\text{neg}}, \\ ((j_b|_{(0, \phi_{\text{infl}})})')^{-1}(-q) & \text{if } q_{\text{neg}} < q < \bar{q}, \\ \phi_{\text{infl}} & \text{if } q \geq \bar{q}. \end{cases}$$

For $q_{\text{neg}} < q < 0$, there is a zero of $j(\cdot; q)$ which we denote by $\phi_Z = \phi_Z(q) \in (0, 1)$. For a specific zone flux functions j_k , we use the notation $\phi_k^M = \phi^M(q_k)$ and $\phi_{kZ} = \phi_M(q_k)$.

In a similar way, one can define the local minimum point, greater than the inflection point, for $0 \leq q < \bar{q}$. We denote it by $\phi_{kM} = \phi_M(q_k)$. For $q \geq \bar{q}$, we define $\phi_{kM}(q) := \phi_{\text{infl}}$. Furthermore, for a given ϕ_{kM} , we define ϕ_{km} as the unique value that satisfies

$$j_k(\phi_{km}; q) = j_k(\phi_{kM}; q), \quad 0 \leq \phi_{km} \leq \phi_{\text{infl}}. \quad (4.3)$$

Analogous definitions can be made for the flux functions $f_k(\cdot, \phi, t)$, $k = 1, 2$.

4.4 Construction of steady states

We seek piecewise smooth and piecewise monotone steady-state solutions $\phi = \phi(z)$ of (1.2). Such solutions may contain jump discontinuities within or between the zones. In the case $D \equiv 0$, Bürger et al. (2019) outlined the details on how to construct unique steady-state solutions and we will not go through the entire machinery here. The basic idea is to glue together solutions within each zone in a unique way so that the conservation of mass holds across the zone borders. Two such so-called Rankine-Hugoniot conditions (jump conditions) are (3.10) and (3.11). Since each such equation has two unknowns; for example, ϕ_E^- and ϕ_E^+ in (3.10), another so-called entropy condition in the theory of degenerate parabolic PDEs with spatially discontinuous coefficients is needed to establish a unique pair of boundary values (Diehl, 2009). Furthermore, as the values ϕ_E^- and ϕ_E^+ are obtained, these are substituted into (3.11) and a similar procedure yields φ_E^- and φ_E^+ .

The new ingredient due to the drainage is the term $\partial_z D(\phi)|_{z=z_E^-}$ in (3.10) and (3.11). The property (1.4) implies the following (see Evje & Karlsen (2000); Diehl (2009) for further details). A discontinuity of the solution $\phi(\cdot, t)$, within or between zones, is possible only between two values in the

interval $0 \leq \phi \leq \phi_c$. Furthermore, since we are seeking piecewise smooth and piecewise monotone steady-state solutions, the fact $d(\phi) > 0$ implies that if one of the values of the discontinuity is ϕ_c , this must be the larger value and located on the right; i.e., the left value of the jump $\phi^- < \phi_c$. Furthermore, $j_2(\phi) \geq j_2(\phi_c)$ for $\phi^- \leq \phi \leq \phi_c$, and in a right neighbourhood of the jump, $\phi'(z) \geq 0$.

With these facts in mind, we now construct steady-state solutions. Let $H(z)$ denote the Heaviside function and assume that all volumetric flows and feed volume fractions are time independent. A stationary solution $\phi = \phi(z)$ of (1.2) satisfies, in the weak sense,

$$\frac{d}{dz} \left(A(z) \left(J(\phi, z) - \gamma(z) \frac{dD(\phi)}{dz} \right) - Q_F \phi_F H(z - z_F) \right) = 0, \quad z \in \mathbb{R}.$$

Integrating this identity with respect to z yields

$$A(z) \left(J(\phi, z) - \gamma(z) d(\phi) \phi'(z) \right) - Q_F \phi_F H(z - z_F) = \mathcal{M}, \quad z \in \mathbb{R}, \quad (4.4)$$

where the constant mass flux \mathcal{M} can be determined by setting z to a value either less than z_U or greater than z_E ; then one gets

$$\begin{aligned} \mathcal{M} &= A_U j_U(\phi_U) = -Q_U \phi_U, \\ \mathcal{M} &= A_E j_E(\phi_E) - Q_F \phi_F =: \mathcal{M}_E - Q_F \phi_F, \end{aligned}$$

where the effluent constant mass flux of aggregates $\mathcal{M}_E := A_E j_E(\phi_E) = Q_E \phi_E$ is also the constant mass flux above the feed inlet. For a desired steady state satisfying (4.1), we have $\phi_U = 0$; hence, $\mathcal{M} = 0$ and the feed mass flux equals the effluent:

$$\phi_U = 0 \quad \Leftrightarrow \quad Q_F \phi_F = \mathcal{M}_E.$$

It is convenient to define the feed mass flux per area unit by

$$s_F := \frac{Q_F \phi_F}{A_E}. \quad (4.5)$$

With z in zone 2, (4.4) gives $\mathcal{M} = A_E (j_2(\phi) - D(\phi)') - Q_F \phi_F$, which with $\mathcal{M} = 0$ and (4.5) implies that the solution ϕ in zone 2 satisfies

$$\begin{aligned} j_2(\phi) - d(\phi) \phi'(z) &= s_F, \quad z_F < z < z_E, \\ s_F &= q_E \phi_E. \end{aligned} \quad (4.6)$$

The boundary condition in (4.6) also implies that ϕ_E can be expressed in terms of given and control variables (recall that $Q_E > 0$):

$$\phi_E = \frac{A_E s_F}{Q_E} = \frac{Q_F \phi_F}{Q_W + Q_F - Q_U}. \quad (4.7)$$

Since we require that there be no aggregates in zone 1, the steady-state solution there is zero. For any jump across $z = z_F$ from this zero volume fraction to any larger value $\bar{\phi}_2$, from which there should be a discontinuity in zone 2 at $z = z_{fr}$, the bottom of the froth layer, the uniqueness condition (Diehl, 2009) implies that $\bar{\phi}_2$ has to lie on an increasing part of $j_2(\cdot; q_2)$. This corresponds to cases (a) and (c) in (Bürger et al., 2019, Section 3.2). The latter case can only occur under special circumstances with a large $\bar{\phi}_2 > \phi_{2M}$ (see definition in Section 4.3). Any small disturbance in a volumetric flow will make the

case impossible and we therefore ignore that case. Consequently, we consider only $\bar{\phi}_2 \in [0, \phi_2^M]$. Then $\bar{\phi}_2$ is the smallest positive solution of the jump condition equation at the feed level, namely

$$s_F = j_2(\bar{\phi}; q_2), \quad (\text{FJC})$$

under the conditions (Bürger et al., 2019)

$$s_F \leq j_2(\phi_2^M; q_2), \quad (\text{FIa})$$

$$\bar{\phi}_2 \leq \phi_{1Z}, \quad (\text{FIb})$$

where ϕ_2^M and ϕ_{1Z} are defined in Section 4.3. By the properties of j_2 , we have $\phi_2^M \leq \phi_{\text{infl}} < \phi_c$. Therefore, $\bar{\phi}_2 < \phi_2^M < \phi_c$. Then $d(\bar{\phi}_2) = 0$, and the equation in (4.6) reduces to (FJC). Again with reference to Diehl (2009) and without going into details, we claim that the solution in zone 2 is

$$\phi_2(z) = \begin{cases} \bar{\phi}_2, & z_F < z < z_E, & \text{if } \phi_E \leq \phi_c, \\ \bar{\phi}_2, & z_F < z < z_{\text{fr}}, & \text{if } \phi_E > \phi_c \text{ and } z_{\text{fr}} > z_F, \\ \phi_{2\text{par}}(z), & z_{\text{fr}} < z \leq z_E, & \end{cases} \quad (4.8)$$

where $\phi_{2\text{par}}(z)$ is the strictly increasing solution of the ordinary differential equation (see (4.6)):

$$\phi'(z) = \frac{j_2(\phi; q_2) - s_F}{d(\phi)}, \quad (4.9)$$

$$\phi(z_{\text{fr}}) = \phi_c, \quad \phi(z_E) = \phi_E,$$

and where z_{fr} is the unknown location of the pulp-froth interface $\phi = \phi_c$, which depends on s_F and ϕ_E .

See Figure 4.3 for illustrations of some steady-state solutions in zone 2. In (4.8) lies the fact that if $\phi_E > \phi_c$, then there is no discontinuity at $z = z_E$, so that $\phi_{2\text{par}}(z_E^-) = \phi_E^- = \phi_E^+ = \phi_E$. The boundary value problem (4.9) defines a function Z_{fr} via

$$z_{\text{fr}} = Z_{\text{fr}}(\phi_F, Q_F, Q_U, Q_W).$$

In light of (4.7) and (4.8), necessary conditions for a steady-state solution with a froth region are the inequalities

$$\phi_c < \phi_E \leq 1 \quad \Leftrightarrow \quad Q_F \left(1 - \frac{\phi_F}{\phi_c}\right) < Q_U - Q_W \leq Q_F(1 - \phi_F), \quad (\text{Froth1})$$

$$z_F < Z_{\text{fr}}(\phi_F, Q_F, Q_U, Q_W) \quad (\text{Froth2})$$

that should be satisfied for a steady-state solution with a froth-pulp interface in zone 2. The requirement that $\phi_{2\text{par}}(z)$ is strictly increasing from ϕ_c to ϕ_E means that the left inequality of (Froth1) is equivalent to $Z_{\text{fr}}(\phi_F, Q_F, Q_U, Q_W) < z_E$; hence, the latter inequality need not be invoked.

That $\phi_{2\text{par}}(z)$ is strictly increasing, required by the entropy condition in Diehl (2009), means that the right-hand side of (4.9) is positive in the interval $[\phi_c, \phi_E]$. Furthermore, a discontinuity at $z = z_{\text{fr}}$ from $\bar{\phi}_2$ up to ϕ_c can only occur (according to the entropy condition) if the graph of $j_2(\cdot; q_2)$ lies above s_F in the interval $(\bar{\phi}_2, \phi_c)$. These conditions imply (FIa), which we can abandon. The properties of $j_2(\cdot; q_2)$ (see Section 4.3) imply that we can write these necessary conditions for a solution with a froth region:

$$s_F < j_2(\phi; q_2) \quad \text{for all } \phi \in (\phi_2^M, \phi_E) \quad \Leftrightarrow \quad s_F \begin{cases} < j_2(\phi_{2M}; q_2) & \text{if } \phi_{2M} < \phi_E, \\ \leq j_2(\phi_E; q_2) & \text{if } \phi_{2M} \geq \phi_E, \end{cases} \quad (\text{Froth3})$$

where equality holds if and only if $\phi_{2M} = \phi_E$.

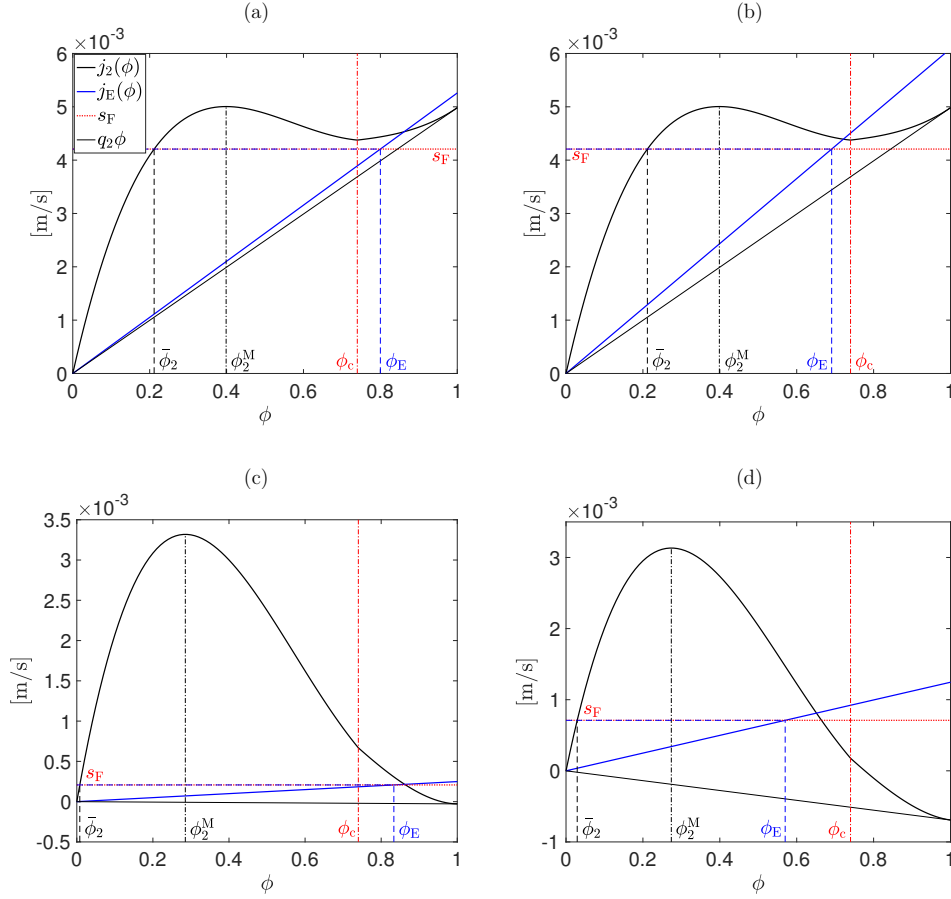


FIG. 4.3. Possible steady-state values for zone 2 with (a, b) $q_2 > 0$ and (c, d) $q_2 < 0$. The case $\phi_E > \phi_c$ is shown in (a) and (c), where there is a continuously increasing solution $\phi_{\text{par}}(z) \in (\phi_c, \phi_E)$, while $\phi_E \leq \phi_c$ in (b) and (d), where the solution in zone 2 is the constant $\bar{\phi}_2$. For all the cases, we have $\phi_c = 0.74$, $n_b = 2.5$ and $n_S = 0.46$. For (a) and (b), $Q_2 := q_2 A_E = 3.6 \times 10^{-5} \text{ m}^3/\text{s}$, $s_F = 4.21 \times 10^{-3} \text{ m/s}$ and (a) $Q_W = 2 \times 10^{-6} \text{ m}^3/\text{s}$, (b) $Q_W = 8 \times 10^{-6} \text{ m}^3/\text{s}$. For (c) we let $Q_2 = -2 \times 10^{-6} \text{ m}^3/\text{s}$, $Q_W = 2 \times 10^{-6} \text{ m}^3/\text{s}$ and $s_F = 2.07 \times 10^{-4} \text{ m/s}$, while for (d) we used $Q_2 = -5 \times 10^{-6} \text{ m}^3/\text{s}$, $Q_W = 10^{-5} \text{ m}^3/\text{s}$ and $s_F = 7.1 \times 10^{-4} \text{ m/s}$.

4.5 Desired steady states and operating charts

From the derivation above concerning the aggregates and from the treatment in Bürger et al. (2019) concerning the solids, we here summarize the *desired steady states* that satisfy (4.1):

$$\phi_{\text{SS}}(z) = \begin{cases} 0 & \text{for } z_U < z < z_F, \\ \bar{\phi}_2 & \text{for } z_F < z < z_{\text{fr}}, \\ \phi_{2\text{par}}(z) & \text{for } z_{\text{fr}} < z < z_E, \\ \phi_E & \text{for } z > z_E, \end{cases} \quad (4.10)$$

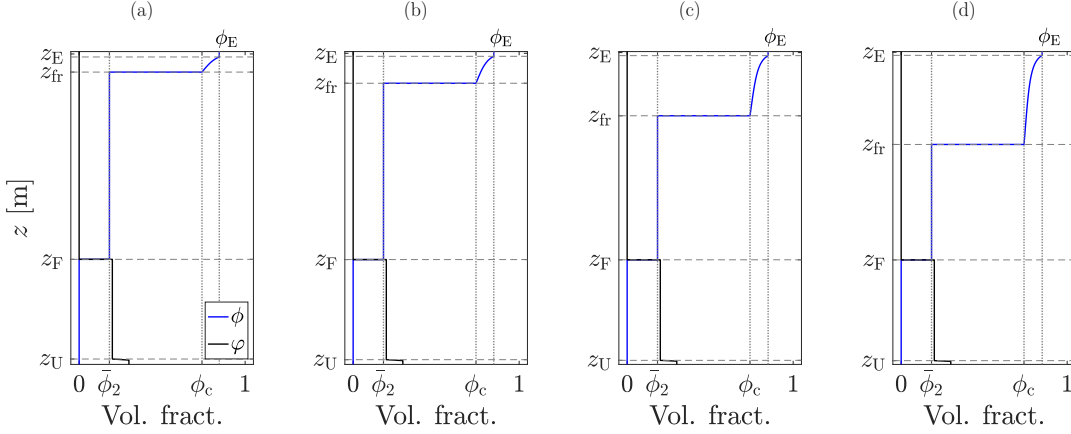


FIG. 4.4. Examples of desired steady states given by (4.10) and (4.11). We use fixed values of $\phi_F = 0.3$, $\psi_F = 0.2$, $Q_F = 8.9927 \times 10^{-5} \text{ m}^3/\text{s}$ and $Q_W = 2 \times 10^{-6} \text{ m}^3/\text{s}$ and vary Q_U , choosing: (a) $Q_U = 5.9972 \times 10^{-5} \text{ m}^3/\text{s}$, (b) $Q_U = 6.0083 \times 10^{-5} \text{ m}^3/\text{s}$, (c) $Q_U = 6.0155 \times 10^{-5} \text{ m}^3/\text{s}$ and (d) $Q_U = 6.0171 \times 10^{-5} \text{ m}^3/\text{s}$. Once the values of ϕ_F , Q_U , Q_F and Q_W are chosen, the values of the effluent concentration ϕ_E are given by (4.7) and used as input in the ODE (4.9) to calculate the value of z_{fr} . In particular, we get (a) $\phi_E = 0.8443$, (b) $\phi_E = 0.8472$, (c) $\phi_E = 0.8491$ and (d) $\phi_E = 0.8495$. The values of ϕ_F , ψ_F , Q_U , Q_F and Q_W chosen here are used in Example 1 in Section 6 to recover these profiles using the numerical method proposed in Section 5.

$$\varphi_{SS}(z) = \begin{cases} 0 & \text{for } z > z_F, \\ \varphi_1 \in [0, \varphi_{1m}] & \text{for } z_U < z < z_F, \\ \varphi_U = \varphi_1 + A_U f_b(\varphi_1)/Q_U & \text{for } z < z_U. \end{cases} \quad (4.11)$$

Here, $\phi_{2\text{par}}(z)$ is the solution of the ODE problem (4.9), ϕ_E is given by (4.7), φ_{1m} is given by (4.3) and $\varphi_1 > 0$ satisfies the jump condition at the feed level $z = z_F$ (φ_1 is unique if condition (FIas) below holds; see Bürger et al. (2019))

$$Q_F \psi_F = A_U f_1(\varphi_1, 0; q_1). \quad (\text{FICs})$$

In Figure 4.4, we have represented some examples of desired steady states with different values of z_{fr} obtained by fixing the values of the parameters ϕ_F , ψ_F , Q_F and Q_W and choosing different values for Q_U . As it can be seen, the location of z_{fr} is very sensitive to the choice of Q_U . For instance, it changes from $z_{fr} = 0.8027 \text{ m}$ in (c) to $z_{fr} = 0.7081 \text{ m}$ in (d) with a small variation in Q_U of $-1.6 \times 10^{-8} \text{ m}^3/\text{s}$. We now collect the conditions for obtaining a desired steady state in terms of the input and control variables.

THEOREM 4.1 The desired steady-state solution (4.10) and (4.11) of the PDE system (1.2) is possible only if the following inequalities are satisfied:

$$\bar{\phi}_2 \leq \phi_Z(-Q_U/A_U), \quad (\text{FIb})$$

$$A_U f_1(\varphi_M(-Q_U/A_U), 0; -Q_U/A_U) \geq Q_F \psi_F. \quad (\text{FIas})$$

$$Q_F \left(1 - \frac{\phi_F}{\phi_c}\right) < Q_U - Q_W \leq Q_F(1 - \phi_F), \quad (\text{Froth1})$$

$$z_F < Z_{fr}(\phi_F, Q_F, Q_U, Q_W), \quad (\text{Froth2})$$

$$s_F \begin{cases} < j_2(\phi_{2M}; q_2) & \text{if } \phi_{2M} < \phi_E, \\ \leq j_2(\phi_E; q_2) & \text{if } \phi_{2M} \geq \phi_E, \end{cases} \quad (\text{Froth3})$$

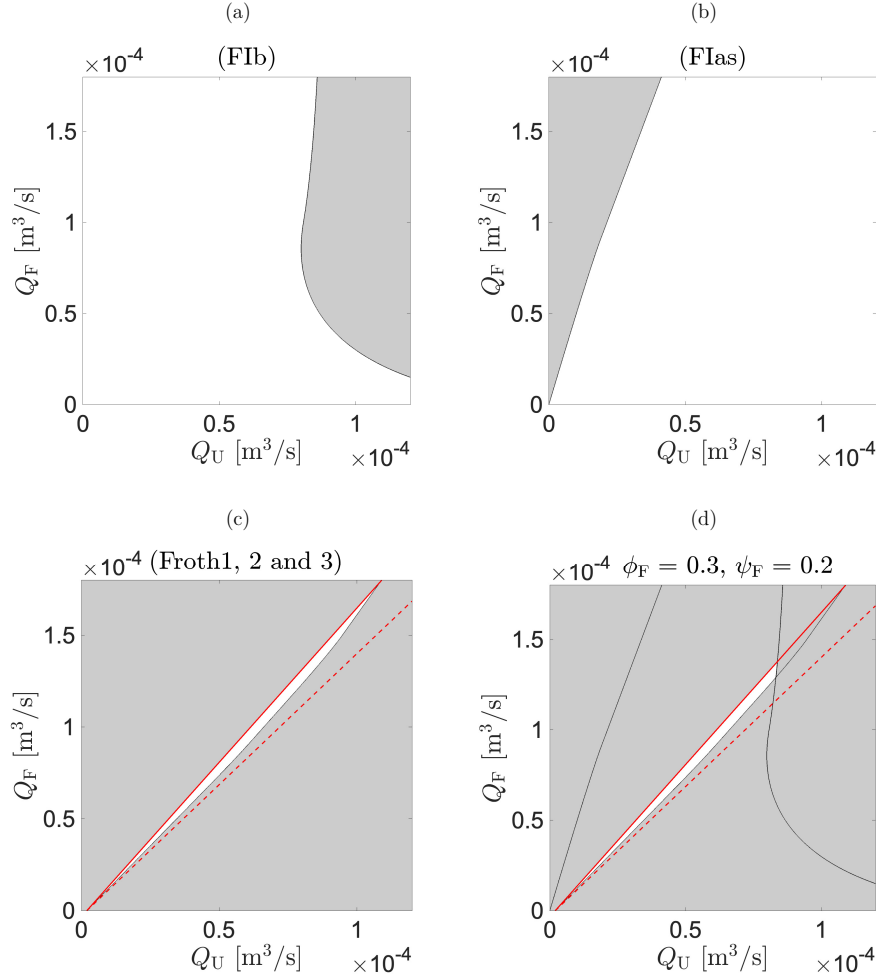


FIG. 4.5. (a–c) Visualization of the conditions of Theorem 4.1 for $Q_W = 2 \times 10^{-6} \text{ m}^3/\text{s}$, $\phi_F = 0.3$ and $\psi_F = 0.2$. (d) Operating chart showing the intersection of all the conditions, which are true in the white region.

where we recall the definitions of q_2 (3.6) and ϕ_E (4.7):

$$q_2 = \frac{-Q_U + Q_F}{A_E}, \quad \phi_E = \frac{Q_F \phi_F}{Q_W + Q_F - Q_U}.$$

Inequalities (FIb) and (FIas) can also be found in (Bürger et al., 2019). We visualize them together with (Froth1), (Froth2) and (Froth3) in the (Q_U, Q_F) -plane for fixed values of Q_W , ϕ_F , ψ_F and z_F ; see Figure 4.5 for the choices $Q_W = 2 \times 10^{-6} \text{ m}^3/\text{s}$, $\phi_F = 0.3$, $\psi_F = 0.2$, and $z_F = 0.33 \text{ m}$. All the conditions are shown together in Figure 4.5 (d), which we call an *operating chart*. For any chosen point (Q_U, Q_F) in the white region, where all conditions in Theorem 4.1 are satisfied, a desired steady-state solution given by (4.10) and (4.11) can be reached.

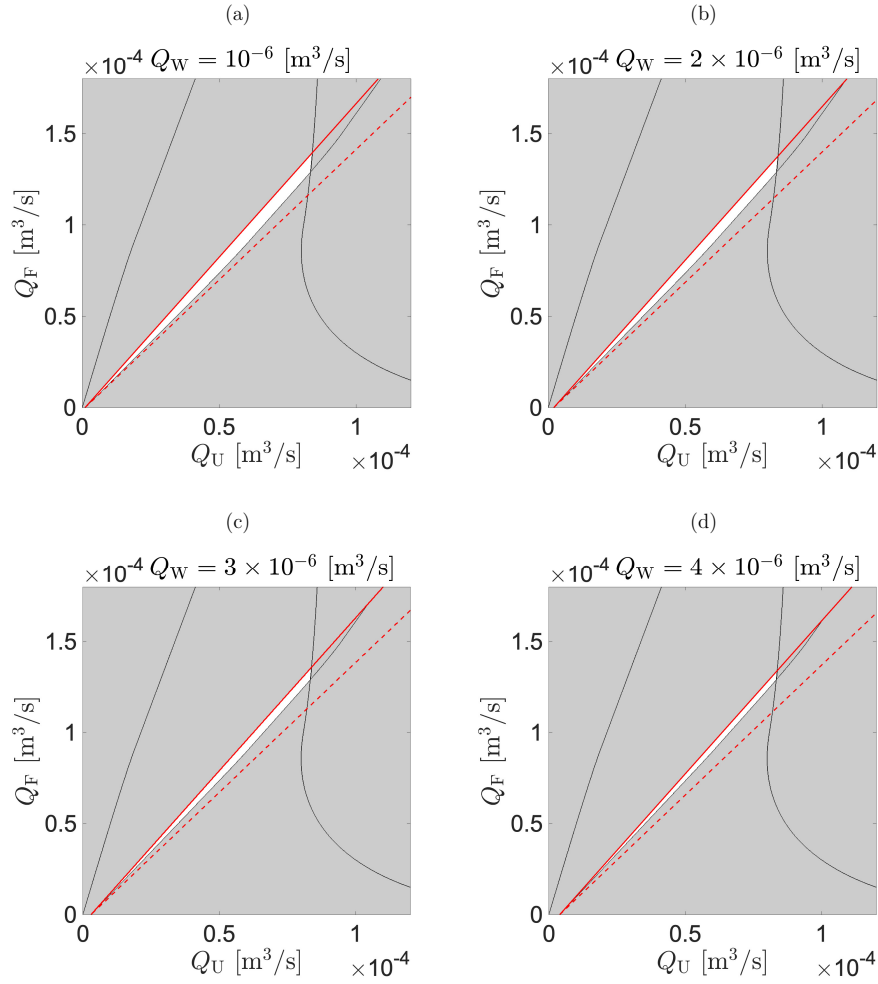


FIG. 4.6. Dependence of the operating chart on the wash water flow Q_W for $\phi_F = 0.3$ and $\psi_F = 0.2$.

The two inequalities in (Froth1) give rise to a wedge-shaped region with vertex at $(Q_U, Q_F) = (Q_W, 0)$; see Figure 4.5 (c). Thus, each wedge displayed in Figure 4.6 corresponds to a fixed value of Q_W , which can be read off at its vertex on the Q_U -axis. The strict inequality of (Froth1) corresponds to the lower dashed line of a wedge, and its slope is positive or negative depending on whether ϕ_F is greater or less than ϕ_c . The difference in slope of the two lines is $\phi_F(1/\phi_c - 1)$, so the angle of the wedge increases with ϕ_F and decreases with ϕ_c . The lower part of the wedge is, however, cut off by conditions (Froth2) and (Froth3); see Figure 4.5 (c). Figure 4.6 shows also that the white region of the operating chart thins and will eventually disappear as Q_W increases.

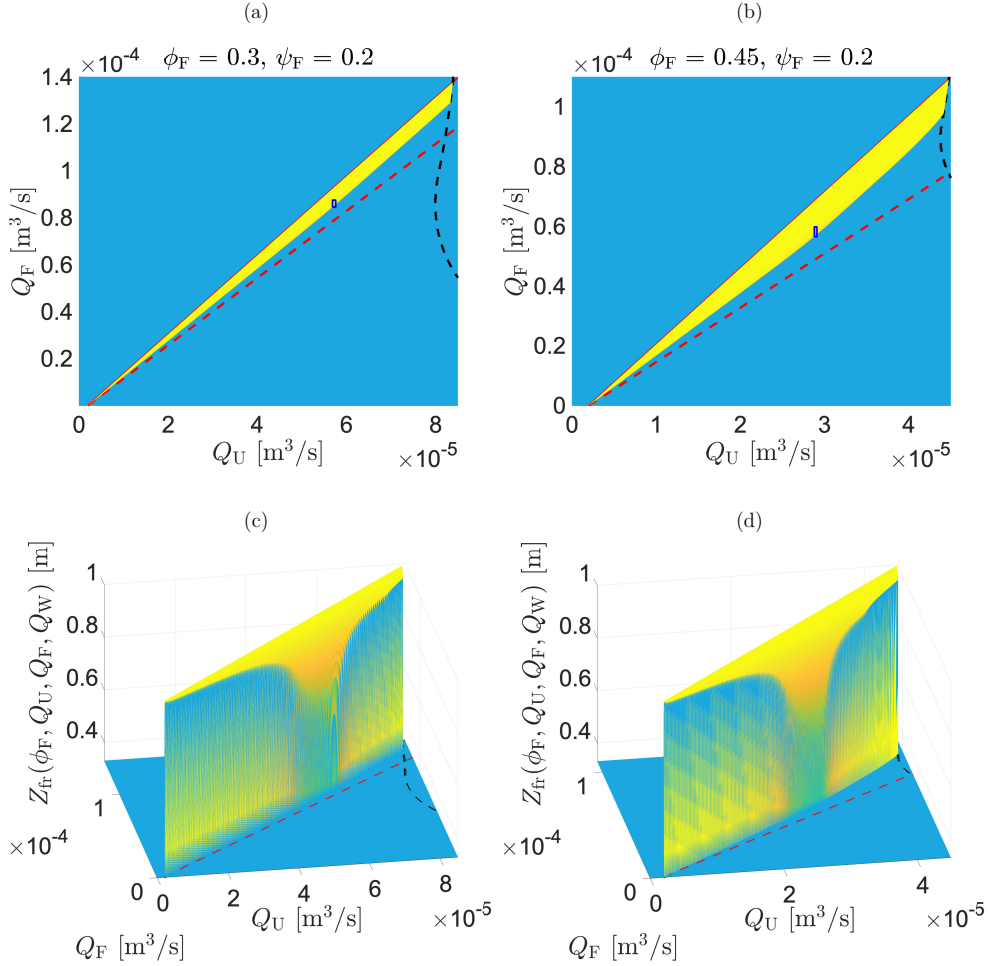


FIG. 4.7. Operating charts for $Q_W = 2 \times 10^{-6} \text{ m}^3/\text{s}$ and $\psi_F = 0.2$ with (a, c) $\phi_F = 0.3$ and (b, d) $\phi_F = 0.45$, showing the graphs of $(Q_F, Q_U) \mapsto Z_{fr}(\phi_F, Q_U, Q_F, Q_W)$ obtained by (4.9). The small rectangles in (a, b) are enlarged in Figure 4.8.

Inequality (Froth2) is more involved than the others. For every given set of input and control values, one has to integrate the ODE of (4.9) backwards from $z = z_E$ for given ϕ_E towards lower z -values until ϕ_c is reached; the corresponding location defines $z = z_{fr}$. In Figure 4.7, the surface $z = Z_{fr}(\phi_F, Q_U, Q_F, Q_W)$ has been computed for two different values of ϕ_F and fixed values of Q_W and ψ_F . The same red and black curves as in Figures 4.5 and 4.6 of conditions (Froth1) and (Flb), respectively, limit the white region in the operating charts. The study of the surface $Z_{fr}(\phi_F, Q_U, Q_F, Q_W)$ is crucial for the choice of values of Q_F , Q_U and Q_W for which we obtain a desired steady state with a froth region in $z = z_{fr}$, with z_{fr} a given value, as we will see in the numerical results in Section 6.

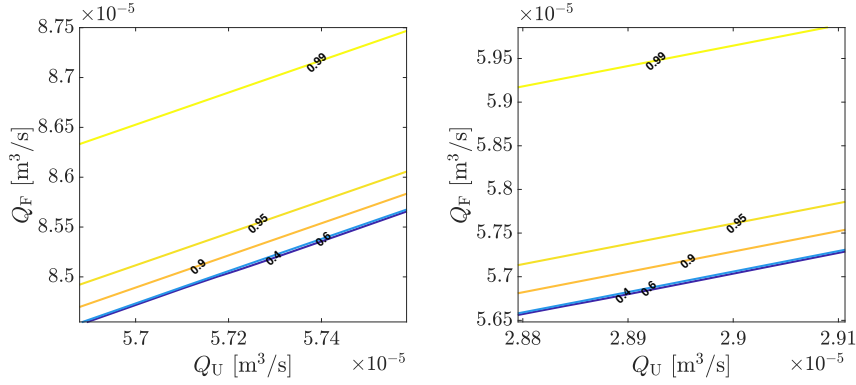


FIG. 4.8. Enlarged views of the small rectangles marked in Figure 4.7 (a) and (b), respectively, showing contours of the function $(Q_F, Q_U) \mapsto Z_{fr}(\phi_F, Q_F, Q_U, Q_W)$.

5. Numerical method

5.1 Discretization and CFL condition

We define a computational domain of N cells by covering the vessel with $N - 2$ cells and placing one cell each below and above for the calculation of the outlet volume fractions see Figure 5.1. Given the column height H , we define $\Delta z := H/(N - 2)$ and the cell boundaries $z_i := i\Delta z$, $i = 0, 1, \dots, N$. Furthermore, we define the cell intervals $I_{i-1/2} := [z_{i-1}, z_i]$ and $I_i := [z_{i-1/2}, z_{i+1/2})$. We place the column between $z_U := \Delta z = z_1$ and $z_E := z_U + H = (N - 1)\Delta z = z_{N-1}$. The injection point z_F is assumed to belong to one cell $I_{i-1/2}$ and we define the dimensionless function

$$\delta_{F,i-1/2} := \int_{I_{i-1/2}} \delta_{z_F}(z) dz := \begin{cases} 1 & \text{if } z_F \in I_{i-1/2}, \\ 0 & \text{otherwise.} \end{cases}$$

The cross-sectional area $A = A(z)$ is allowed to have a finite number of discontinuities and it is discretized by

$$A_i := \frac{1}{\Delta z} \int_{I_i} A(z) dz, \quad A_{i+1/2} := \frac{1}{\Delta z} \int_{I_{i+1/2}} A(z) dz.$$

We simulate N_T time steps up to the final time $T := N_T \Delta t$, with the fixed time step Δt satisfying the Courant-Friedrichs-Lewy (CFL) condition

$$\Delta t \left(\frac{2\|Q\|_{\infty,T}}{A_{\min}} + M_1 \|\tilde{v}'\|_{\infty} + \max\{\beta_1, \beta_2\} \right) \leq \Delta z, \quad (\text{CFL})$$

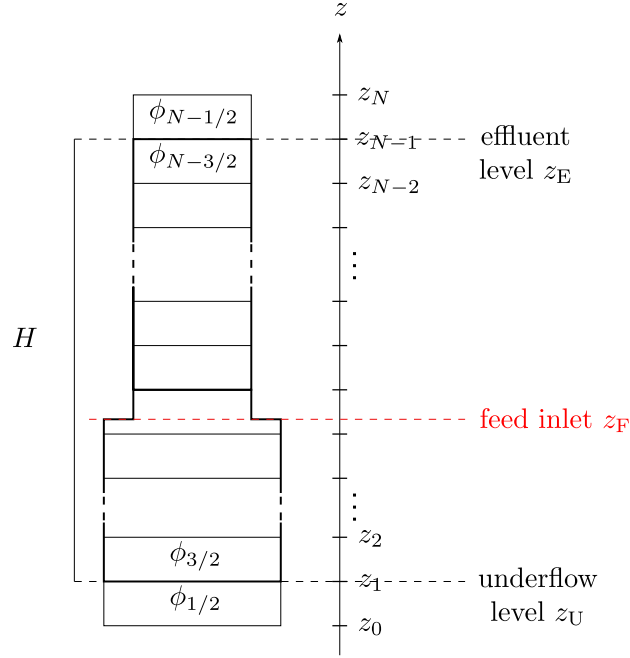


FIG. 5.1. Grid covering the flotation column for the discretization of ϕ and ψ . The outlets z_U and z_E are each fixed on the boundaries between two cells and the feed inlet z_F is then located in a cell.

where

$$\beta_1 := M_1 \|\tilde{v}\|_\infty + M_2 \frac{\|d\|_\infty}{\Delta z}, \quad \beta_2 := M_1 \max \{v_{hs}(0), \|v'_{hs}\|_\infty\} + M_2(1 - \phi_c) \frac{\|d\|_\infty}{\Delta z},$$

$$M_1 := \max_{i=1,2,\dots,N} \left\{ \frac{A_{i-1}}{A_{i-1/2}}, \frac{A_i}{A_{i-1/2}} \right\}, \quad M_2 := \max_{i=1,2,\dots,N} \left\{ \frac{A_{i-1} + A_i}{A_{i-1/2}} \right\},$$

$$A_{\min} := \min_{k=0, \frac{1}{2}, 1, \frac{3}{2}, \dots, N} A_k, \quad \|Q\|_{\infty, T} := \max_{0 \leq t \leq T} (Q_F(t) + Q_W(t)), \quad \|d\|_\infty := \max_{0 \leq \phi \leq 1} |d(\phi)|.$$

Finally, we set $t^n := n\Delta t$ for $n = 0, 1, \dots, N_T$.

The time-dependent feed functions are discretized as

$$Q_F^n := \frac{1}{\Delta t} \int_{t^n}^{t^{n+1}} Q_F(t) dt, \quad \phi_F^n := \frac{1}{\Delta t} \int_{t^n}^{t^{n+1}} \phi_F(t) dt,$$

and the same is made for ψ_F .

5.2 Update of ϕ

The first equation of (1.2) depends only on ϕ and is discretized by a simple scheme on the cells $I_{i-1/2}$. The initial data are discretized by

$$\phi_{i-1/2}^0 := \frac{1}{A_{i-1/2} \Delta z} \int_{I_{i-1/2}} \phi(z, 0) A(z) dz.$$

To advance from t^n to t^{n+1} , we assume that $\phi_{i-1/2}^n$, $i = 1, \dots, N$, are given. With the notation

$$a^+ := \max\{a, 0\}, \quad a^- := \min\{a, 0\}, \quad \gamma_i := \gamma(z_i), \quad \text{and} \quad q_i^{n+} := q(z_i, t^n)^+,$$

we define the numerical total flux at $z = z_i$ at time $t = t^n$ by

$$\Phi_i^n := \begin{cases} \phi_{1/2}^n q_0^{n-} & \text{for } i = 0, \\ \phi_{i-1/2}^n q_i^{n+} + \phi_{i+1/2}^n q_i^{n-} + \gamma_i \phi_{i-1/2}^n \tilde{v}(\phi_{i+1/2}^n) - \gamma_i \frac{D(\phi_{i+1/2}^n) - D(\phi_{i-1/2}^n)}{\Delta z} & \text{for } i = 1, \dots, N-1, \\ \phi_{N-1/2}^n q_N^{n+} & \text{for } i = N, \end{cases} \quad (5.1)$$

where $\tilde{v}(\phi)$ is defined by (3.1). Since the bulk fluxes above and below the tank are directed away from it, the following terms that appear in (5.1) are zero:

$$\phi_{-1/2}^n q_0^{n+} = 0 \quad \text{and} \quad \phi_{N+1/2}^n q_N^{n-} = 0 \quad \text{for any values of } \phi_{-1/2}^n \text{ and } \phi_{N+1/2}^n.$$

To simplify the presentation, we use the middle line of (5.1) as the definition of Φ_i^n , $i = 0, \dots, N$, together with $\phi_{-1/2}^n := 0$ and $\phi_{N+1/2}^n := 0$. With the notation $\lambda := \Delta t / \Delta z$ and $\mathcal{Q}_i^{n+} := A_i q_i^{n+}$ etc., the conservation law on the interval $I_{i-1/2}$ implies the update formula

$$\begin{aligned} \phi_{i-1/2}^{n+1} &= \phi_{i-1/2}^n + \frac{\lambda}{A_{i-1/2}} (A_{i-1} \Phi_{i-1}^n - A_i \Phi_i^n + \mathcal{Q}_F^n \delta_{F,i-1/2}) \\ &= \phi_{i-1/2}^n + \frac{\lambda}{A_{i-1/2}} \left(\phi_{i-3/2}^n \mathcal{Q}_{i-1}^{n+} + \phi_{i-1/2}^n \mathcal{Q}_{i-1}^{n-} + (A\gamma)_{i-1} \phi_{i-3/2}^n \tilde{v}(\phi_{i-1/2}^n) \right. \\ &\quad \left. - \frac{(A\gamma)_{i-1}}{\Delta z} (D(\phi_{i-1/2}^n) - D(\phi_{i-3/2}^n)) - \phi_{i-1/2}^n \mathcal{Q}_i^{n+} - \phi_{i+1/2}^n \mathcal{Q}_i^{n-} - (A\gamma)_i \phi_{i-1/2}^n \tilde{v}(\phi_{i+1/2}^n) \right. \\ &\quad \left. + \frac{(A\gamma)_i}{\Delta z} (D(\phi_{i+1/2}^n) - D(\phi_{i-1/2}^n)) + \mathcal{Q}_F^n \delta_{F,i-1/2} \right), \quad i = 1, \dots, N. \end{aligned} \quad (5.2)$$

THEOREM 5.1 If the CFL condition (CFL) is satisfied and the initial data satisfy $0 \leq \phi(z, 0) \leq 1$, then the update formula for ϕ , (5.2), is monotone and produces approximate solutions that satisfy

$$0 \leq \phi_{i-1/2}^n \leq 1 \quad \text{for } i = 1, \dots, N \text{ and } n = 1, \dots, N_T. \quad (5.3)$$

The proof is outlined in Appendix A.

5.3 Update of ψ

We discretize the initial data by

$$\psi_{i-1/2}^0 := \frac{1}{A_{i-1/2} \Delta z} \int_{I_{i-1/2}} \psi(z, 0) A(z) dz.$$

A consistent numerical flux corresponding to (3.7) is, for $i = 0, \dots, N$,

$$\Psi_i^n := \psi_{i-1/2}^n q_i^{n+} + \psi_{i+1/2}^n q_i^{n-}$$

$$- \gamma_i \left(G_i^n(\Psi_{i-1/2}^n, \Psi_{i+1/2}^n) + \frac{\Psi_{i+1/2}^n}{1 - \phi_{i+1/2}^n} \left(\phi_{i-1/2}^n \tilde{v}(\phi_{i+1/2}^n) - \frac{\Delta D_i^{n-}}{\Delta z} \right) - \frac{\Psi_{i-1/2}^n}{1 - \phi_{i-1/2}^n} \frac{\Delta D_i^{n+}}{\Delta z} \right),$$

where $\Delta D_i^n := D(\phi_{i+1/2}^n) - D(\phi_{i-1/2}^n)$, $\Delta D_i^{n-} := (\Delta D_i^n)^-$, and we set

$$\Psi_{-1/2}^n := 0 \quad \text{and} \quad \Psi_{N+1/2}^n := 0$$

with the same motivation as for ϕ above (these values are irrelevant). Here $G_i^n(\Psi_{i-1/2}^n, \Psi_{i+1/2}^n)$ is the Engquist-Osher numerical flux (Engquist & Osher, 1981) associated with the function

$$f_{b,i}^n(\Psi) := \Psi \tilde{v}_{\text{hs}} \left(\frac{\Psi}{\Psi_{\max,i}^n} \right), \quad \tilde{v}_{\text{hs}}(u) := \begin{cases} v_{\text{hs}}(u) & \text{for } u < 1, \\ 0 & \text{for } u \geq 1, \end{cases} \quad (5.4)$$

where we recall that v_{hs} is given by (3.5), and we define

$$\Psi_{\max,i}^n := \min\{1 - \phi_{i-1/2}^n, 1 - \phi_{i+1/2}^n\} = 1 - \max\{\phi_{i-1/2}^n, \phi_{i+1/2}^n\}. \quad (5.5)$$

If $\hat{\Psi}_i^n$ is the maximum point of $f_{b,i}^n$, then the Engquist-Osher numerical flux is given by

$$G_i^n(\Psi_{i-1/2}^n, \Psi_{i+1/2}^n) = \begin{cases} f_{b,i}^n(\Psi_{i+1/2}^n) & \text{if } \Psi_{i-1/2}^n, \Psi_{i+1/2}^n \leq \hat{\Psi}_i^n, \\ f_{b,i}^n(\hat{\Psi}_i^n) & \text{if } \Psi_{i-1/2}^n \leq \hat{\Psi}_i^n < \Psi_{i+1/2}^n, \\ -f_{b,i}^n(\hat{\Psi}_i^n) + f_{b,i}^n(\Psi_{i-1/2}^n) + f_{b,i}^n(\Psi_{i+1/2}^n) & \text{if } \Psi_{i+1/2}^n \leq \hat{\Psi}_i^n < \Psi_{i-1/2}^n, \\ f_{b,i}^n(\Psi_{i-1/2}^n) & \text{if } \hat{\Psi}_i^n < \Psi_{i-1/2}^n, \Psi_{i+1/2}^n. \end{cases}$$

The marching formula is (for $i = 1, \dots, N$)

$$\begin{aligned} & \Psi_{i-1/2}^{n+1} \\ &= \Psi_{i-1/2}^n + \frac{\lambda}{A_{i-1/2}} (A_{i-1} \Psi_{i-1}^n - A_i \Psi_i^n + Q_F^n \Psi_F^n \delta_{F,i-1/2}) \\ &= \Psi_{i-1/2}^n + \frac{\lambda}{A_{i-1/2}} \left\{ \Psi_{i-3/2}^n Q_{i-1}^{n+} + \Psi_{i-1/2}^n Q_{i-1}^{n-} - \Psi_{i-1/2}^n Q_i^{n+} - \Psi_{i+1/2}^n Q_i^{n-} + Q_F^n \Psi_F^n \delta_{F,i-1/2} \right. \\ & \quad \left. - (A\gamma)_{i-1} \left(G_{i-1}^n(\Psi_{i-3/2}^n, \Psi_{i-1/2}^n) + \frac{\Psi_{i-1/2}^n}{1 - \phi_{i-1/2}^n} \left(\phi_{i-3/2}^n \tilde{v}(\phi_{i-1/2}^n) - \frac{\Delta D_{i-1}^{n-}}{\Delta z} \right) - \frac{\Psi_{i-3/2}^n}{1 - \phi_{i-3/2}^n} \frac{\Delta D_{i-1}^{n+}}{\Delta z} \right) \right. \\ & \quad \left. + (A\gamma)_i \left(G_i^n(\Psi_{i-1/2}^n, \Psi_{i+1/2}^n) + \frac{\Psi_{i+1/2}^n}{1 - \phi_{i+1/2}^n} \left(\phi_{i-1/2}^n \tilde{v}(\phi_{i+1/2}^n) - \frac{\Delta D_i^{n-}}{\Delta z} \right) - \frac{\Psi_{i-1/2}^n}{1 - \phi_{i-1/2}^n} \frac{\Delta D_i^{n+}}{\Delta z} \right) \right\}. \end{aligned} \quad (5.6)$$

THEOREM 5.2 Assume that the assumptions of Theorem 5.1 are in effect. If the initial data satisfy $0 \leq \psi(z, 0) \leq 1 - \phi(z, 0)$ and the feed volume fraction $\Psi_F(t) \leq 1 - \phi_F(t)$, then the update formula (5.6) is monotone and together with (5.2) it produces approximate solutions that satisfy

$$0 \leq \Psi_{i-1/2}^n \leq 1 - \phi_{i-1/2}^n \quad \text{for all } i \text{ and } n.$$

The proof is sketched in Appendix A.

6. Numerical simulations

We simulate the flotation process in the column in Figure 1.1 with the specific measures $A_E = 7.225 \times 10^{-3} \text{ m}^2 \leq A_U = 8.365 \times 10^{-3} \text{ m}^2$, $z_U = 0 \text{ m}$, $z_F = 0.33 \text{ m}$, $z_E = 1 \text{ m}$ and $H = 1 \text{ m}$. For all the examples, we use the parameters given in (Brito-Parada et al., 2012, Table 1) to define v_{drain} and d_{cap} in (3.1)–(3.3): $\rho_f = 10^3 \text{ kg/m}^3$, $\mu = 10^{-3} \text{ Pa s}$, $r_b = 4.13 \times 10^{-4} \text{ m}$, $C_{\text{PB}} = 50$, $\gamma_w = 3.5 \times 10^{-2} \text{ N/m}$, $g = 9.81 \text{ m/s}^2$, and by Stevenson & Stevanov (2004), $n_S = 0.46$ and $m = 1.28$, from which we obtain $d_{\text{cap}} = 3.1045 \times 10^{-3} \text{ m}$. For the velocity functions \tilde{v} and v_{hs} , given by (3.1) and (3.5), respectively, we use $n_b = 2.5$, $v_{\text{term}} = 2.7 \times 10^{-2} \text{ m/s}$, $n_{\text{RZ}} = 1.5$ and $v_{\infty} = 5.0 \times 10^{-3} \text{ m/s}$. The critical volume fraction is $\phi_c = 0.74$ according to (Neethling & Cilliers, 2003, Eq. (21)).

6.1 Example 1

We show steady-state solutions for fixed $Q_F = 8.9927 \times 10^{-5} \text{ m}^3/\text{s}$ and $Q_W = 2.0 \times 10^{-6} \text{ m}^3/\text{s}$ for various values of Q_U ; see Figure 6.1(a). For these values and with the feed volume fractions $\phi_F = 0.3$ and $\psi_F = 0.2$, we solve the ODE (4.9) to obtain ‘exact’ solutions (i.e., the ODE is solved numerically), and the value of z_{fr} for each point; see the solid lines in Figure 6.1(c) and (d). The dots in the same plots show the numerical solutions, which are obtained by simulating a long time from any initial data. All solutions have the same volume fraction ϕ_E at the top, since this is given by the explicit formula (4.7). Figure 6.1(b) shows the steady state for the solids with particles only below the feed level.

A clear difference between the two types of solution of ϕ can be seen near the discontinuity. This is an inaccuracy of the numerical solution, which seems to converge to the exact one as $N \rightarrow \infty$; see Figure 6.2, which shows the steady-state solution for the solid point in Figure 6.1(a) for various values of N .

6.2 Example 2

We start from a tank filled with only water at time $t = 0 \text{ s}$, i.e., $\phi(z, 0) = \psi(z, 0) = 0$ for all z , when we start pumping aggregates, solids, fluid and wash water with $\phi_F = 0.3$ and $\psi_F = 0.2$. In the white region of the operating chart in Figure 6.3, we choose the point (diamond symbol) $(Q_U, Q_F) = (5.85, 8.846) \times 10^{-5} \text{ m}^3/\text{s}$. The wash water volumetric flow is $Q_W = 2.0 \times 10^{-6} \text{ m}^3/\text{s}$. Then $Q_E = 1.4496 \times 10^{-4} \text{ m}^3/\text{s}$ and one obtains a desired steady state with a thin layer of froth at the top and solids only below the feed level after about 500 s; see Figures 6.4 (a) and 6.5 (a).

Once the system is in steady state at $t = 500 \text{ s}$, we perform two different changes corresponding to the points marked with a square (left) and a circle (right) in the operating chart in Figure 6.3 with the corresponding responses seen in Figures 6.4 and 6.5, respectively. The jump from the middle point (diamond) to the left point (square) means a jump from $Q_U = 5.85 \times 10^{-5} \text{ m}^3/\text{s}$ to the smaller value $5.0 \times 10^{-5} \text{ m}^3/\text{s}$ and produces the solution in Figure 6.4. After $t = 1000 \text{ s}$, there is no froth in zone 2 and the solids volume fraction is slightly higher in the new steady state.

If the jump from the middle point (diamond) instead goes to the right point (circle), i.e., the new value at $t = 500 \text{ s}$ is the larger $Q_U = 6.3 \times 10^{-5} \text{ m}^3/\text{s}$, Figure 6.5 shows the reaction of the system until $t = 2000 \text{ s}$. The aggregates fill the entire column while the solids volume fraction has a lower value

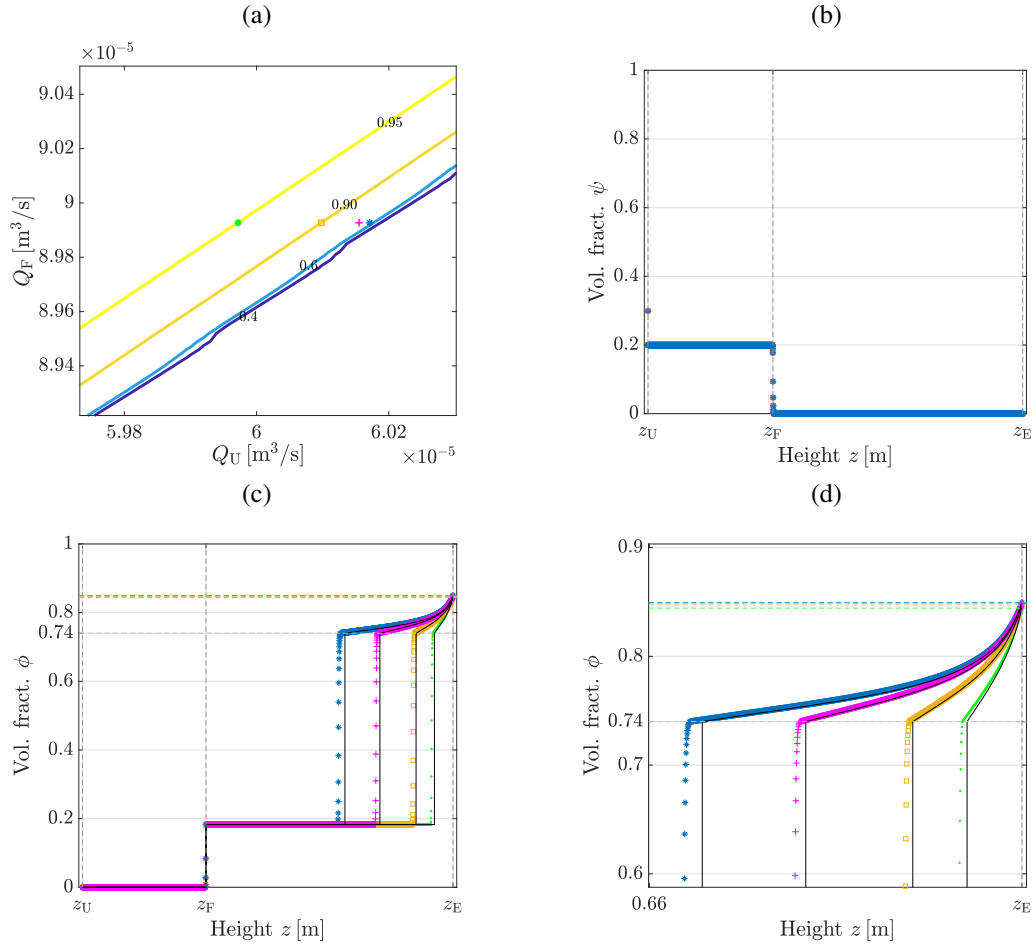


FIG. 6.1. Example 1: (a) Contour lines of $(Q_F, Q_U) \mapsto Z_{fr}(\phi_F, Q_F, Q_U, Q_W)$ for $Q_W = 2 \times 10^{-6} \text{ m}^3/\text{s}$, $\psi_F = 0.2$ and $\phi_F = 0.3$. (b) Approximate volume fraction of solids ψ computed with $N = 3200$. (c) Approximate solution (dots) versus exact solution (solid lines) of volume fraction of aggregates ϕ corresponding to the four point in plot (a) computed with $N = 3200$. (d) Enlarged view of (c).

in the new steady state. We have demonstrated that operating points outside the white region lead to non-desired steady states.

6.3 Example 3

Again, the tank is filled with only water at time $t = 0 \text{ s}$ when we start feeding it with $\phi_F = 0.3$ and $\psi_F = 0.2$. The wash water flow is $Q_W = 4.0 \times 10^{-6} \text{ m}^3/\text{s}$ and hence the effluent volumetric flow is $Q_E = 1.75 \times 10^{-5} \text{ m}^3/\text{s}$. From the corresponding operating chart in Figure 6.6 (a), we choose the point of volumetric flows $(Q_U, Q_F) = (3.15, 4.5) \times 10^{-5} \text{ m}^3/\text{s}$ lying in the white region. Then a desired steady state builds up quickly and at $t = 250 \text{ s}$ there is a thin froth layer at the top of in zone 2 and with solids only in zone 1; see Figure 6.7.

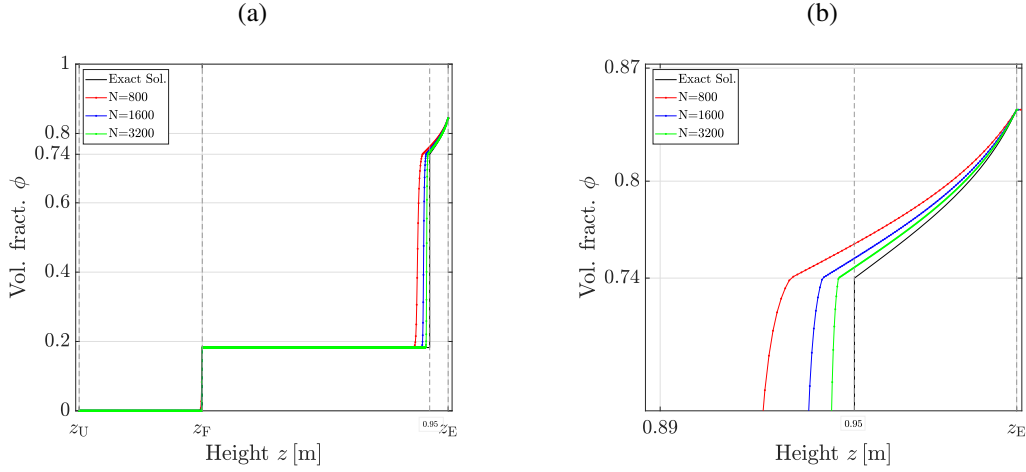


FIG. 6.2. Example 1: (a) Approximate solution for the point represented by a dot in Figure 6.1(a) with various values of N . (b) Enlarged view of (a).

Once the system is in steady state, we change at $t = 300$ s the volumetric flow of the wash water from $Q_W = 4.0 \times 10^{-6} \text{ m}^3/\text{s}$ to $1.0 \times 10^{-6} \text{ m}^3/\text{s}$ and simulate the reaction of the system. In the corresponding operating chart for this new set of variables, the point $(Q_U, Q_F) = (3.15, 4.5) \times 10^{-5} \text{ m}^3/\text{s}$ is no longer in the white region; see Figure 6.6 (b, circle point), and no desired steady state is feasible. As it can be seen in Figure 6.7 (a), with less flow of wash water flushing the aggregates out at the top, the froth layer increases downwards. At time $t = 1000$ s, we make a control action and change the volumetric flow from $Q_U = 3.15 \times 10^{-5} \text{ m}^3/\text{s}$ to $3.0 \times 10^{-5} \text{ m}^3/\text{s}$ so that the new point lies inside the white region of the corresponding operating chart in Figure 6.6 (b, diamond point). Figures 6.7 (a) and (c) show that a second desired steady state is reached after $t = 1500$ s. Figures 6.7 (b) and (d) show that the solids settle in any case.

7. Conclusions

Our previous one-dimensional model of a flotation column, where the movement of rising aggregates and settling solids follow the drift- and solids-flux theories, is a triangular hyperbolic 2×2 system of nonlinear PDEs of the first order. Here, we propose an extended model where the drainage of liquid in the froth layer due to capillarity is included. The traditional derivation of the drainage PDE, valid only within the froth, is combined with further experimental findings from the literature to end up in a constitutive relationship between the relative velocity of aggregates to fluid (or suspension of hydrophilic solids), which in the governing equations yields a second-order-derivative degenerate nonlinear term.

An analysis of the possible steady states with a froth layer at the top of the column (desired steady states) leads to several inequalities involving the feed input variables and other control volumetric flows; see Theorem 4.1. Those inequalities are visualized in operating charts; see Figure 4.6, in which the white region shows the necessary location of an operating point (Q_U, Q_F) for having a desired steady state after a time of transient behaviour.

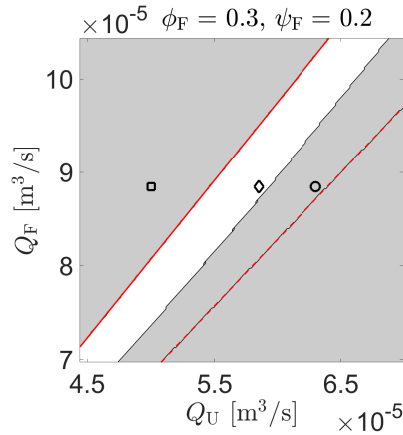


FIG. 6.3. Example 2: An operating chart for $\phi_F = 0.3$ and $\psi_F = 0.2$. The point $(Q_U, Q_F) = (5.85, 8.846) \times 10^{-5} \text{ m}^3/\text{s}$ marked with a diamond in the white region results in a desired steady state with a froth layer at the top of the column. The points marked with a square $(Q_U, Q_F) = (5.0, 8.846) \times 10^{-5} \text{ m}^3/\text{s}$ and a circle $(Q_U, Q_F) = (6.3, 8.84) \times 10^{-5} \text{ m}^3/\text{s}$ result in no froth (Figure 6.4) or a tank full of froth (Figure 6.5), respectively. (The plot is a zoom of Figure 4.6 (b) and the black curves are smoother than they here appear due to numerical resolution.)

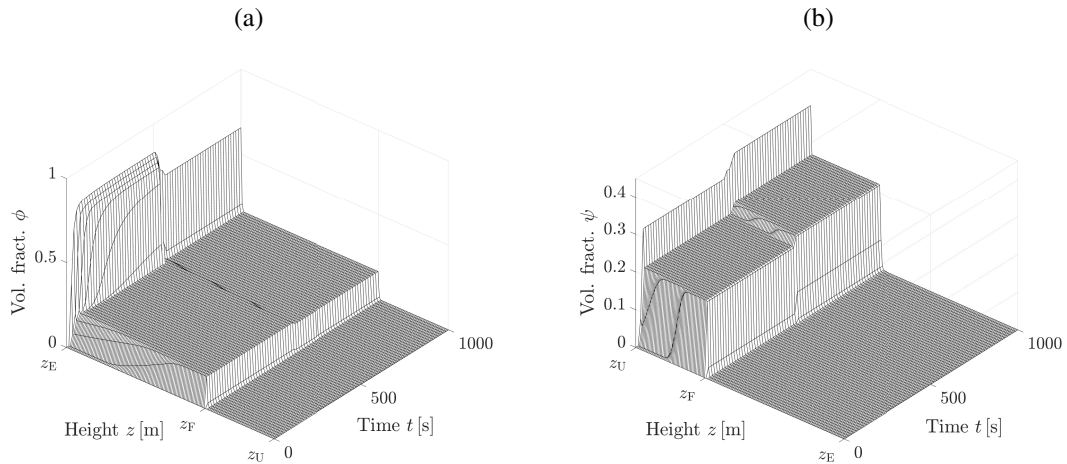


FIG. 6.4. Example 2: Simulation with $N = 1600$ of the volume fractions of (a) aggregates ϕ and (b) solids ψ from a tank filled of only water. The initial operating point $(Q_U, Q_F) = (5.85, 8.846) \times 10^{-5} \text{ m}^3/\text{s}$ (diamond in Figure 6.3) is at $t = 500 \text{ s}$ changed to $(5.0, 8.846) \times 10^{-5} \text{ m}^3/\text{s}$ (square in Figure 6.3).

With parameters extracted from the literature, the white region of an operating chart is quite small, meaning that the existence of a froth layer is very sensitive to small changes in any of the control variables Q_U and Q_W . Different operating points (Q_U, Q_F) in the white region give rise to different thicknesses of the froth layer. Unfortunately, our model anticipates a very sensitive dependence of the pulp-froth interface location z_{fr} on the operating point; see Figure 4.7, where the yellow surface shows that the most common values of z_{fr} is close to one, meaning a thin froth layer. The surfaces

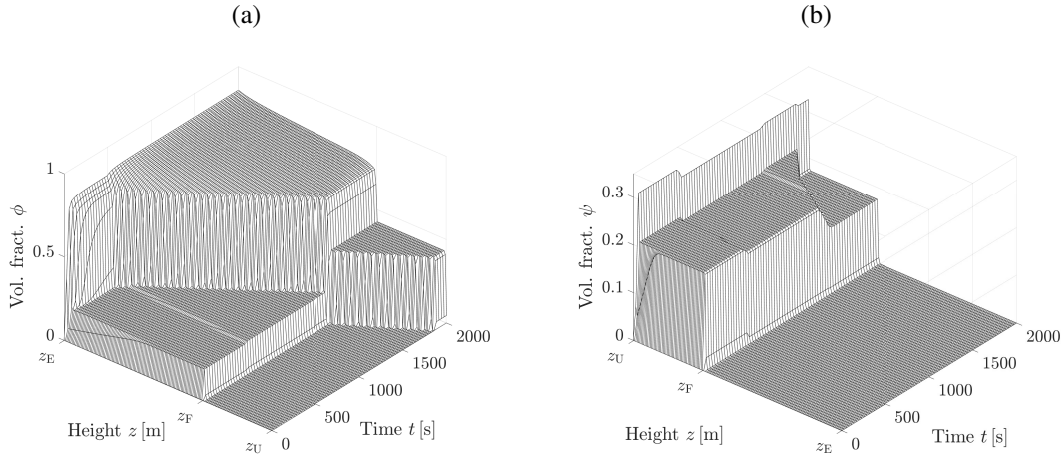


FIG. 6.5. Example 2: Simulation with $N = 1600$ of the volume fractions of (a) aggregates ϕ and (b) solids ψ from a tank filled of only water. The initial operating point $(Q_U, Q_F) = (5.85, 8.846) \times 10^{-5} \text{ m}^3/\text{s}$ (diamond in Figure 6.3) is at $t = 500 \text{ s}$ changed to $(6.3, 8.846) \times 10^{-5} \text{ m}^3/\text{s}$ (circle in Figure 6.3).

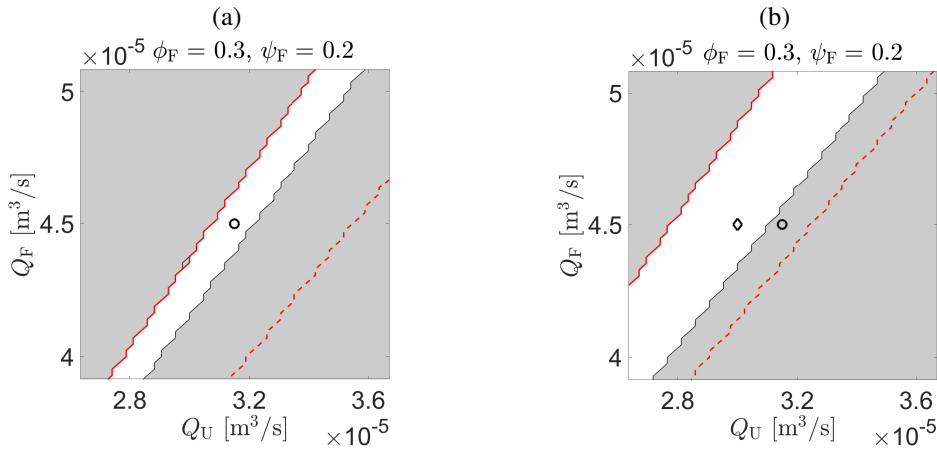


FIG. 6.6. Example 3. Operating charts for $\phi_F = 0.3$ and $\psi_F = 0.2$ with (a) $Q_W = 3.15 \times 10^{-5} \text{ m}^3/\text{s}$, (b) $Q_W = 3.0 \times 10^{-5} \text{ m}^3/\text{s}$. The initial point $(Q_U, Q_F) = (3.15, 4.5) \times 10^{-5} \text{ m}^3/\text{s}$ is marked with a circle and the one after the control action $(Q_U, Q_F) = (3.0, 4.5) \times 10^{-5} \text{ m}^3/\text{s}$ with a diamond. (The curves are smoother than they appear here due to numerical resolution.)

seen in plots (c) and (d) indicate a very large gradient from z_{fr} just below one down to $z_{fr} = 0.33 = z_F$. (Even finer resolutions indicate that the graph is continuous.) The numerical scheme suggested resolves discontinuities well and numerical results (e.g., those of Figure 6.5) show that the volume fractions, and their sum, stay between zero and one, as is proven in Theorems 5.1 and 5.2.

Overall, the steady-state analysis, boundedness properties of the numerical solutions, and simulation results indicate that the model is useful for the simulation of flotation columns and could be used, for example, to simulate the effect of various alternative control actions. In light of this practical interest

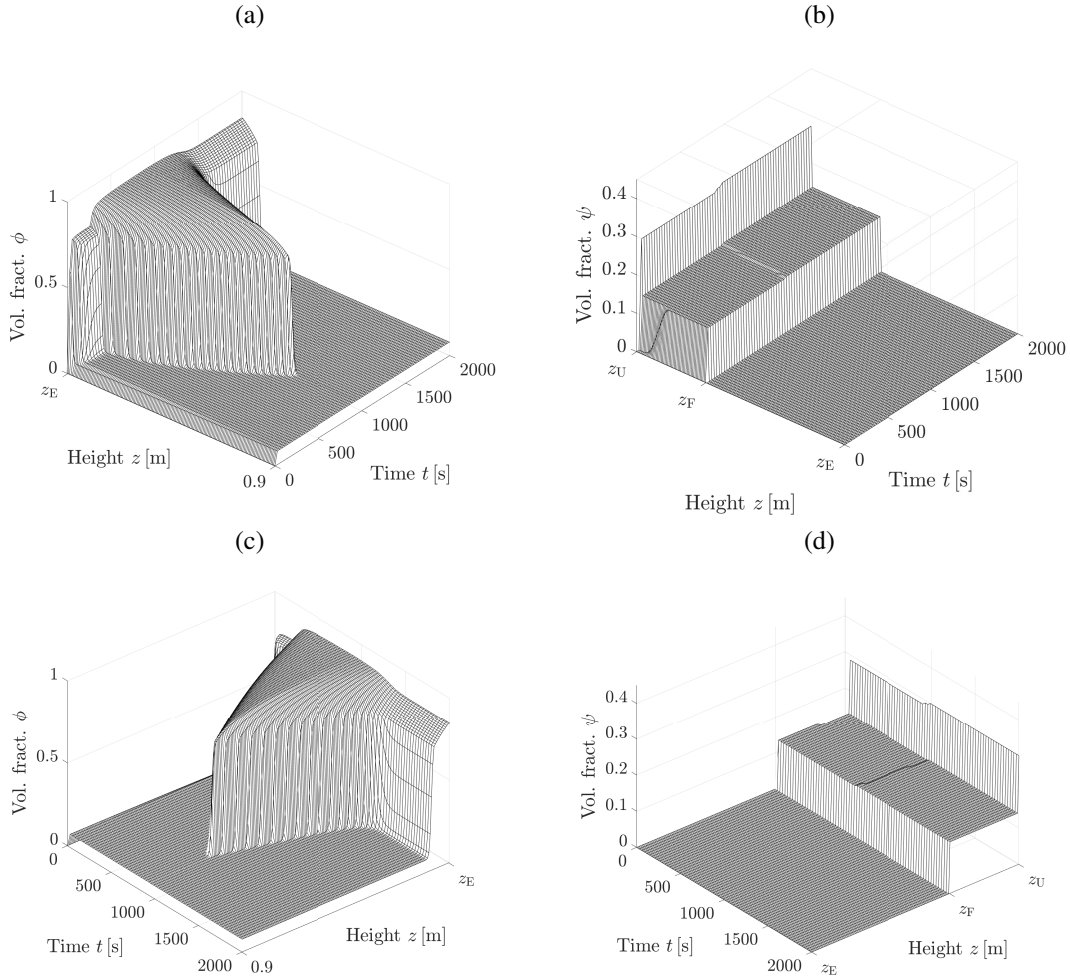


FIG. 6.7. Example 3: Time evolution of the volume fraction (a, c) of aggregates ϕ and (b,d) solids ψ computed with $N = 1600$ and seen from two different angles. A step change down in Q_W occurs at $t = 300$ s and a control action by decreasing Q_U is made at $t = 1000$ s.

it would be desirable to obtain a well-posedness (existence and uniqueness) result for the underlying model. The first equation of (1.2) (the one for ϕ) as a scalar strongly degenerate parabolic equation with discontinuous flux that is independent of ψ can be handled by known arguments (cf., e.g., Karlsen et al. (2002, 2003); Bürger et al. (2005)). The corresponding model for $D \equiv 0$ (without capillarity) is a triangular system of conservation laws for which convergence results of monotone schemes to a weak solution are available, at least for the case of fluxes without spatial discontinuity (Karlsen et al., 2008; Coclite et al., 2010). It is not clear at the moment whether the corresponding arguments, based on the compensated compactness method, can also be applied to the system (1.2). Therefore, well-posedness of the model is at the moment left as an open problem.

The model of a flotation column with drainage can certainly be extended to include additional pro-

cesses. For instance, one could incorporate the possibility of bursting bubbles at the top by assuming that the flotation column is constructed in a way such that a portion α of the froth overflows with unbursting aggregates, whereas for the portion $1 - \alpha$, the aggregates burst. The latter means that the gas ‘disappears’ (i.e., is released into the surrounding air), whereas the suspension and the hydrophobic particles attached to the bursting bubbles follow the effluent stream. There is practical interest in quantifying this effect (Neethling & Brito-Parada, 2018). Hence, the effluent volume fraction of aggregates would then be $\phi_E := \alpha\phi_E^+$, and the solids $\varphi_E := \varphi_E^+$. Under the present assumptions, the factor α does not influence the solution inside the column. It could however depend on the wash water flow, and this could be an extension of the present model. Another thinkable extension could consist in the explicit description of the aggregation process itself. A common variant of the column drawn in Figure 1.1 has gas feed and pulp feed at different levels, which form a so-called collection zone where the attachment of hydrophobic particles takes place. Such a description would compel a distinction between hydrophobic and hydrophilic particles as distinct solid phases.

Acknowledgements

R.B. acknowledges support from ANID (Chile) through Fondecyt project 1210610; Anillo project ANID/PIA/210030; Centro de Modelamiento Matemático (CMM), projects ACE210010 and FB210005 of BASAL funds for Centers of Excellence; and CRHIAM, project ANID/FONDAP/15130015. S.D. acknowledges support from the Swedish Research Council (Vetenskapsrådet, 2019-04601). M.C.M. is supported by grant MTM2017-83942 funded by Spanish MINECO and by grant PID2020-117211GB-I00 funded by MCIN/AEI/10.13039/501100011033. Y.V. is supported by SENACYT (Panama).

REFERENCES

- Ata, S. (2012) Phenomena in the froth phase of flotation — A review. *Int. J. Miner. Process.*, **102-103**, 1–12.
- Azhin, M., Popli, K., Afacan, A., Liu, Q. & Prasad, V. (2021a) A dynamic framework for a three phase hybrid flotation column. *Miner. Eng.*, **170**, 107028.
- Azhin, M., Popli, K. & Prasad, V. (2021b) Modelling and boundary optimal control design of hybrid column flotation. *Can. J. Chem. Eng.*, **99**(S1).
- Bascur, O. A. (1991) A unified solid/liquid separation framework. *Fluid/Particle Sep. J.*, **4**(2), 117–122.
- Brennen, C. E. (2005) *Fundamentals of Multiphase Flow*. Cambridge University Press.
- Bruto-Parada, P. R., Neethling, S. J. & Cilliers, J. J. (2012) The advantages of using mesh adaptivity when modelling the drainage of liquid in froths. *Miner. Eng.*, **33**, 80–86.
- Bürger, R., Diehl, S. & Martí, M. C. (2018) A conservation law with multiply discontinuous flux modelling a flotation column. *Networks Heterog. Media*, **13**(2), 339–371.
- Bürger, R., Diehl, S. & Martí, M. C. (2019) A system of conservation laws with discontinuous flux modelling flotation with sedimentation. *IMA J. Appl. Math.*, **84**(5), 930–973.
- Bürger, R., Diehl, S., Martí, M. C. & Vásquez, Y. (2020a) Flotation with sedimentation: Steady states and numerical simulation of transient operation. *Miner. Eng.*, **157**, 106419.
- Bürger, R., Diehl, S., Martí, M. C. & Vásquez, Y. (2020b) Simulation and control of dissolved air flotation and column froth flotation with simultaneous sedimentation. *Water Sci. Tech.*, **81**(8), 1723–1732.
- Bürger, R., Diehl, S., Martí, M. C. & Vásquez, Y. (2022) A difference scheme for a triangular system of conservation laws with discontinuous flux modeling three-phase flows. In preparation.
- Bürger, R., Karlsen, K. H., Risebro, N. H. & Towers, J. D. (2004) Well-posedness in BV_t and convergence of a difference scheme for continuous sedimentation in ideal clarifier-thickener units. *Numer. Math.*, **97**, 25–65.
- Bürger, R., Karlsen, K. H. & Towers, J. D. (2005) A model of continuous sedimentation of flocculated suspensions in clarifier-thickener units. *SIAM J. Appl. Math.*, **65**, 882–940.

- Bürger, R., Wendland, W. L. & Concha, F. (2000) Model equations for gravitational sedimentation-consolidation processes. *Z. Angew. Math. Mech.*, **80**, 79–92.
- Bustos, M. C., Concha, F., Bürger, R. & Tory, E. M. (1999) *Sedimentation and Thickening: Phenomenological Foundation and Mathematical Theory*. Kluwer Academic Publishers, Dordrecht, The Netherlands.
- Coclite, G. M., Mishra, S. & Risebro, N. H. (2010) Convergence of an Engquist-Osher scheme for a multi-dimensional triangular system of conservation laws. *Math. Comp.*, **79**(269), 71–94.
- Cruz, E. B. (1997) *A comprehensive dynamic model of the column flotation unit operation*. PhD thesis, Virginia Tech, Blacksburg, Virginia.
- Dickinson, J. E. & Galvin, K. P. (2014) Fluidized bed desliming in fine particle flotation – Part I. *Chem. Eng. Sci.*, **108**, 283–298.
- Diehl, S. (1996) A conservation law with point source and discontinuous flux function modelling continuous sedimentation. *SIAM J. Appl. Math.*, **56**(2), 388–419.
- Diehl, S. (1997) Dynamic and steady-state behavior of continuous sedimentation. *SIAM J. Appl. Math.*, **57**(4), 991–1018.
- Diehl, S. (2001) Operating charts for continuous sedimentation I: Control of steady states. *J. Eng. Math.*, **41**, 117–144.
- Diehl, S. (2008a) A regulator for continuous sedimentation in ideal clarifier-thickener units. *J. Eng. Math.*, **60**, 265–291.
- Diehl, S. (2008b) The solids-flux theory – confirmation and extension by using partial differential equations. *Water Res.*, **42**(20), 4976–4988.
- Diehl, S. (2009) A uniqueness condition for nonlinear convection-diffusion equations with discontinuous coefficients. *J. Hyperbolic Differential Equations*, **6**, 127–159.
- Ekama, G. A., Barnard, J. L., Günthert, F. W., Krebs, P., McCorquodale, J. A., Parker, D. S. & Wahlberg, E. J. (1997) *Secondary Settling Tanks: Theory, Modelling, Design and Operation*. IAWQ scientific and technical report no. 6. International Association on Water Quality, England.
- Ekama, G. A. & Marais, P. (2004) Assessing the applicability of the 1D flux theory to full-scale secondary settling tank design with a 2D hydrodynamic model. *Water Res.*, **38**, 495–506.
- Engquist, B. & Osher, S. (1981) One-sided difference approximations for nonlinear conservation laws. *Math. Comp.*, **36**(154), 321–351.
- Evje, S. & Karlsen, K. H. (2000) Monotone difference approximations of BV solutions to degenerate convection-diffusion equations. *SIAM J. Numer. Anal.*, **37**, 1838–1860.
- Galvin, K. P. & Dickinson, J. E. (2014) Fluidized bed desliming in fine particle flotation – Part II: Flotation of a model feed. *Chem. Eng. Sci.*, **108**, 299–309.
- Galvin, K. P., Harvey, N. G. & Dickinson, J. E. (2014) Fluidized bed desliming in fine particle flotation – Part III flotation of difficult to clean coal. *Minerals Eng.*, **66-68**, 94–101.
- Gol'dfarb, I. I., Kann, K. B. & Shreiber, I. R. (1988) Liquid flow in foams. *Fluid Dynamics*, **23**(2), 244–249.
- Haffner, B., Khidas, Y. & Pitois, O. (2015) The drainage of foamy granular suspensions. *J. Colloid Interface Sci.*, **458**, 200–208.
- Karlsen, K. H., Mishra, S. & Risebro, N. H. (2008) Convergence of finite volume schemes for triangular systems of conservation laws. *Numer. Math.*, **111**(4), 559–589.
- Karlsen, K. H., Risebro, N. H. & Towers, J. D. (2002) Upwind difference approximations for degenerate parabolic convection-diffusion equations with a discontinuous coefficient. *IMA J. Numer. Anal.*, **22**(4), 623–664.
- Karlsen, K. H., Risebro, N. H. & Towers, J. D. (2003) L^1 Stability for Entropy Solutions of Nonlinear Degenerate Parabolic Convection-Diffusion Equations with Discontinuous Coefficients. *Trans. Royal Norwegian Society Sci. Letters (Skr. K. Nor. Vidensk. Selsk.)*, **3**, 49.
- Koehler, S. A., Hilgenfeldt, S. & Stone, H. A. (2000) A generalized view of foam drainage: Experiment and theory. *Langmuir*, **16**(15), 6327–6341.
- Kynch, G. J. (1952) A theory of sedimentation. *Trans. Faraday Soc.*, **48**, 166–176.

- La Motta, E. J., McCorquodale, J. A. & Rojas, J. A. (2007) Using the kinetics of biological flocculation and the limiting flux theory for the preliminary design of activated sludge systems. I: Model development. *J. Environ. Eng.*, **133**(1), 104–110.
- Leonard, R. A. & Lemlich, R. (1965) Laminar longitudinal flow between close-packed cylinders. *Chem. Eng. Sci.*, **20**(8), 790–791.
- Narsimhan, G. (2010) Analysis of creaming and formation of foam layer in aerated liquid. *J. Colloid Interface Sci.*, **345**(2), 566–572.
- Neethling, S. J. & Brito-Parada, P. R. (2018) Predicting flotation behaviour – The interaction between froth stability and performance. *Miner. Eng.*, **120**, 60–65.
- Neethling, S. J. & Cilliers, J. J. (2002) Solids motion in flowing froths. *Chem. Eng. Sci.*, **57**(4), 607–615.
- Neethling, S. J. & Cilliers, J. J. (2003) Modelling flotation froths. *Int. J. Miner. Proc.*, **72**(1-4), 267–287.
- Neethling, S. J., Lee, H. T. & Cilliers, J. J. (2002) A foam drainage equation generalized for all liquid contents. *J. Physics: Condensed Matter*, **14**(3), 331–342.
- Pal, R. & Masliyah, J. (1989) Flow characterization of a flotation column. *Can. J. Chem. Eng.*, **67**(6), 916–923.
- Quintanilla, P., Neethling, S. J. & Brito-Parada, P. R. (2021) Modelling for froth flotation control: A review. *Minerals Eng.*, **162**, 106718.
- Richardson, J. F. & Zaki, W. N. (1954) Sedimentation and fluidization: part I. *Trans. Inst. Chem. Engineers (London)*, **32**, 35–53.
- Rietema, K. (1982) Science and technology of dispersed two-phase systems—I and II. *Chem. Eng. Sci.*, **37**(8), 1125–1150.
- Stevenson, P. (2006) Dimensional analysis of foam drainage. *Chem. Eng. Sci.*, **61**(14), 4503–4510.
- Stevenson, P., Fennell, P. S. & Galvin, K. P. (2008) On the drift-flux analysis of flotation and foam fractionation processes. *Can. J. Chem. Eng.*, **86**(4), 635–642.
- Stevenson, P. & Stevanov, C. (2004) Effect of rheology and interfacial rigidity on liquid recovery from rising froth. *Ind. Eng. Chem. Res.*, **43**(19), 6187–6194.
- Tian, Y., Azhin, M., Luan, X., Liu, F. & Dubljevic, S. (2018a) Three-phases dynamic modelling of column flotation process. *IFAC-PapersOnLine*, **51**(21), 99–104.
- Tian, Y., Luan, X., Liu, F. & Dubljevic, S. (2018b) Model predictive control of mineral column flotation process. *Mathematics*, **6**(6), 100.
- Vandenbergh, J., Choung, J., Xu, Z. & Masliyah, J. (2005) Drift flux modelling for a two-phase system in a flotation column. *Can. J. Chem. Eng.*, **83**(2), 169–176.
- Verbist, G., Weaire, D. & Kraynik, A. M. (1996) The foam drainage equation. *J. Physics: Condensed Matter*, **8**(21), 3715–3731.
- Wallis, G. B. (1969) *One-Dimensional Two-Phase Flow*. McGraw-Hill, New York. 281 pp.

A. Proofs of boundedness of numerical solutions

We outline the proofs of Theorems 5.1 and 5.2, which are both based on monotonicity arguments. The calculations are straightforward in both cases; details for the case $D \equiv 0$ are provided by Bürger et al. (2022).

Outline of the proof of Theorem 5.1

Assume that $\phi_{i-1/2}^n$ and $\tilde{\phi}_{i-1/2}^n$, $i \in \mathbb{Z}$, $n = 0, 1, 2, \dots$ are two numerical solutions produced by the numerical scheme (5.2). Then monotonicity means that if $\phi_{i-1/2}^n \leq \tilde{\phi}_{i-1/2}^n$ for all i , then $\phi_{i-1/2}^{n+1} \leq \tilde{\phi}_{i-1/2}^{n+1}$ for all i , for all $n = 0, 1, 2, \dots$. For the case of a three-point scheme such as (5.2) this property can be verified

by showing that $\partial\phi_{i-1/2}^{n+1}/\partial\phi_{k-1/2}^n \geq 0$ for all i and $k = i-1, i, i+1$. In fact, we have

$$\begin{aligned} \frac{\partial\phi_{i-1/2}^{n+1}}{\partial\phi_{i-3/2}^n} &= \frac{\lambda}{A_{i-1/2}} \left(Q_{i-1}^{n+} + (A\gamma)_{i-1} (\tilde{v}(\phi_{i-1/2}^n) + d(\phi_{i-3/2}^n)/\Delta z) \right) \geq 0, \\ \frac{\partial\phi_{i-1/2}^{n+1}}{\partial\phi_{i+1/2}^n} &= \frac{\lambda}{A_{i-1/2}} \left(-Q_i^{n-} + (A\gamma)_i (-\phi_{i-1/2}^n \tilde{v}'(\phi_{i+1/2}^n) + d(\phi_{i+1/2}^n)/\Delta z) \right) \geq 0, \\ \frac{\partial\phi_{i-1/2}^{n+1}}{\partial\phi_{i-1/2}^n} &= 1 + \frac{\lambda}{A_{i-1/2}} \left(Q_{i-1}^{n-} + (A\gamma)_{i-1} \phi_{i-3/2}^n \tilde{v}'(\phi_{i-1/2}^n) - Q_i^{n+} - (A\gamma)_i \tilde{v}(\phi_{i+1/2}^n) \right. \\ &\quad \left. - ((A\gamma)_{i-1} + (A\gamma)_i) d(\phi_{i-1/2}^n)/\Delta z \right) \\ &\geq 1 - \lambda \left(\frac{2\|Q\|_{\infty, T}}{A_{\min}} + M_1 (\|\tilde{v}'\|_{\infty} + \|\tilde{v}\|_{\infty}) + M_2 \frac{\|d\|_{\infty}}{\Delta z} \right) \geq 0, \end{aligned}$$

where we have used the CFL condition (CFL). The rest of the proof, the boundedness $0 \leq \phi_{i-1/2}^n \leq 1$, follows by standard arguments, namely one verifies that if $\phi_{i-1/2}^n = 0$ for all i , then $\phi_{i-1/2}^{n+1} = 0$ for all i and likewise that if $\phi_{i-1/2}^n = 1$ for all i , then $\phi_{i-1/2}^{n+1} = 1$ for all i . Thus, appealing to the monotonicity of the scheme, one deduces that if $0 \leq \phi_{i-1/2}^n \leq 1$ for all i , then $0 \leq \phi_{i-1/2}^{n+1} \leq 1$ for all i , which proves (5.3).

Proof of Theorem 5.2

The proof is similar to that of Theorem 5.1. We note that (5.6) is again a three-point scheme, and show that $\partial\psi_{i-1/2}^{n+1}/\partial\psi_{k-1/2}^n \geq 0$ for all $i = 1, \dots, N$ and $k = i-1, i, i+1$. The contributions of the terms that contain D to $\partial\psi_{i-1/2}^{n+1}/\partial\psi_{i-3/2}^n$ and $\partial\psi_{i-1/2}^{n+1}/\partial\psi_{i+1/2}^n$ are

$$\frac{\lambda(A\gamma)_{i-1}}{A_{i-1/2}(1-\phi_{i-3/2}^n)} \frac{\Delta D_{i-1}^{n+}}{\Delta z} \geq 0 \quad \text{and} \quad -\frac{\lambda(A\gamma)_i}{A_{i+1/2}(1-\phi_{i+1/2}^n)} \frac{D_{i-1}^{n-}}{\Delta z} \geq 0,$$

respectively. Now we utilize the estimations similar to those in the previous proof (see Bürger et al. (2022)) and add the terms with D to obtain

$$\begin{aligned} \frac{\partial\mathcal{K}_{i-1/2}^n}{\partial\psi_{i-1/2}^n} &\geq 1 - \lambda \left(\frac{2\|Q\|_{\infty, T}}{A_{\min}} + M_1 (\max\{v_{\text{hs}}(0), \|v'_{\text{hs}}\|_{\infty}\}) + \|\tilde{v}'\|_{\infty} \right) \\ &\quad + \frac{1}{A_{i-1/2}(1-\phi_{i-1/2}^n)} \left((A\gamma)_{i-1} \frac{\Delta D_{i-1}^{n-}}{\Delta z} - (A\gamma)_i \frac{\Delta D_i^{n+}}{\Delta z} \right). \end{aligned}$$

It is easy to estimate the integrated terms

$$\Delta D_i^n = D(\phi_{i+1/2}^n) - D(\phi_{i-1/2}^n) \leq \|d\|_{\infty}(1 - \phi_c).$$

Hence, we obtain with (CFL)

$$\frac{\partial\mathcal{K}_{i-1/2}^n}{\partial\psi_{i-1/2}^n} \geq 1 - \lambda \left(\frac{2\|Q\|_{\infty, T}}{A_{\min}} + M_1 (\max\{v_{\text{hs}}(0), \|v'_{\text{hs}}\|_{\infty}\}) + \|\tilde{v}'\|_{\infty} + M_2(1 - \phi_c) \frac{\|d\|_{\infty}}{\Delta z} \right) \geq 0.$$

The inequalities proven imply that $\psi_{i-1/2}^{n+1}$ is a non-decreasing of each of $\psi_{k-1/2}^n$ for $k = i-1, i, i+1$, and therefore the scheme is monotone. Writing the scheme as

$$\psi_{i-1/2}^{n+1} = \mathcal{K}_{i-1/2}(\psi_{i-3/2}^n, \psi_{i-1/2}^n, \psi_{i+1/2}^n),$$

assuming that $0 \leq \psi_{i-1/2}^n \leq 1 - \phi_{i-1/2}^n$ for all i and using that (5.4) and (5.5) ensure that $G_i^n(1 - \phi_{i-1/2}^n, 1 - \phi_{i+1/2}^n) = 0$ (see Bürger et al. (2022)), we get

$$\begin{aligned} 0 &\leq \frac{\lambda}{A_{i-1/2}} \mathcal{Q}_{\text{F}}^n \psi_{\text{F}}^n \delta_{\text{F},i-1/2} = \mathcal{K}_{i-1/2}(0, 0, 0) \leq \psi_{i-1/2}^{n+1} \\ &= \mathcal{K}_{i-1/2}(\psi_{i-3/2}^n, \psi_{i-1/2}^n, \psi_{i+1/2}^n) \leq \mathcal{K}_{i-1/2}(1 - \phi_{i-3/2}^n, 1 - \phi_{i-1/2}^n, 1 - \phi_{i+1/2}^n) \\ &= 1 - \phi_{i-1/2}^n + \frac{\lambda}{A_{i-1/2}} \left((1 - \phi_{i-3/2}^n) \mathcal{Q}_{i-1}^{n+} + (1 - \phi_{i-1/2}^n) \mathcal{Q}_{i-1}^{n-} \right. \\ &\quad \left. - (\mathcal{A}\gamma)_{i-1} \left(\phi_{i-3/2}^n \tilde{v}(\phi_{i-1/2}^n) - \frac{\Delta D_{i-1}^{n-}}{\Delta z} - \frac{\Delta D_{i-1}^{n+}}{\Delta z} \right) - (1 - \phi_{i-1/2}^n) \mathcal{Q}_i^{n+} - (1 - \phi_{i+1/2}^n) \mathcal{Q}_i^{n-} \right. \\ &\quad \left. + (\mathcal{A}\gamma)_i \left(\phi_{i-1/2}^n \tilde{v}(\phi_{i+1/2}^n) - \frac{\Delta D_i^{n-}}{\Delta z} - \frac{\Delta D_i^{n+}}{\Delta z} \right) + \mathcal{Q}_{\text{F}}^n \psi_{\text{F}}^n \delta_{\text{F},i-1/2} \right). \end{aligned}$$

Now we use that $\Delta D_i^{n-} + \Delta D_i^{n+} = \Delta D_i^n = D(\phi_{i+1/2}) - D(\phi_{i-1/2})$, that $\psi_{\text{F},k}^n \leq 1 - \phi_{\text{F},k}^n$ and the update formula for ϕ (5.2) to obtain

$$\begin{aligned} \psi_{i-1/2}^{n+1} &\leq 1 - \phi_{i-1/2}^{n+1} + \frac{\lambda}{A_{i-1/2}} (\mathcal{Q}_{i-1}^{n+} + \mathcal{Q}_{i-1}^{n-} - \mathcal{Q}_i^{n+} - \mathcal{Q}_i^{n-} + \mathcal{Q}_{\text{F}}^n \delta_{\text{F},i-1/2}) \\ &= 1 - \phi_{i-1/2}^{n+1} + \frac{\lambda}{A_{i-1/2}} (\mathcal{Q}_{i-1}^n - \mathcal{Q}_i^n + \mathcal{Q}_{\text{F}}^n \delta_{\text{F},i-1/2}) = 1 - \phi_{i-1/2}^{n+1}, \end{aligned}$$

since the latter parenthesis is zero irrespective of whether there is a source in the cell; $\mathcal{Q}_{i-1}^n - \mathcal{Q}_i^n + \mathcal{Q}_{\text{F}}^n = 0$, or not; $\mathcal{Q}_{i-1}^n - \mathcal{Q}_i^n = 0$.

Centro de Investigación en Ingeniería Matemática (CI²MA)

PRE-PUBLICACIONES 2021 - 2022

- 2021-25 REINALDO CAMPOS-VARGAS, ESTHER CARRERA, BRUNO G. DEFILIPPI, CLAUDIA FUENTEALBA, IGNACIA HERNÁNDEZ, MAARTEN HERTOOG, CLAUDIO MENESES, GERARDO NUÑEZ, DIEGO PAREDES, ROMINA PEDRESCHI, VIRGILIO UARROTA: *Transcriptome and hormone analyses reveals differences in physiological age of “Hass” avocado fruit*
- 2021-26 TOMÁS BARRIOS, EDWIN BEHRENS, ROMMEL BUSTINZA: *Numerical analysis of a stabilized mixed method applied to incompressible elasticity problems with Dirichlet and with mixed boundary conditions*
- 2021-27 LILIANA CAMARGO, MANUEL SOLANO: *A high order unfitted HDG method for the Helmholtz equation with first order absorbing boundary condition*
- 2021-28 ANA ALONSO-RODRIGUEZ, JESSIKA CAMAÑO: *A graph-based algorithm for the approximation of the spectrum of the curl operator*
- 2021-29 VERONICA ANAYA, RUBEN CARABALLO, RICARDO RUIZ-BAIER, HECTOR TORRES: *Augmented finite element formulation for the Navier-Stokes equations with vorticity and variable viscosity*
- 2021-30 CLAUDIO I. CORREA, GABRIEL N. GATICA: *On the continuous and discrete well-posedness of perturbed saddle-point formulations in Banach spaces*
- 2022-01 NESTOR SÁNCHEZ, TONATIUH SANCHEZ-VIZUET, MANUEL SOLANO: *Afternote to Coupling at a distance: convergence analysis and a priori error estimates*
- 2022-02 GABRIEL N. GATICA, CRISTIAN INZUNZA, FILANDER A. SEQUEIRA: *A pseudostress-based mixed-primal finite element method for stress-assisted diffusion problems in Banach spaces*
- 2022-03 ELIGIO COLMENARES, RICARDO OYARZÚA, FRANCISCO PIÑA: *A fully-DG method for the stationary Boussinesq system*
- 2022-04 JUAN MANUEL CÁRDENAS, MANUEL SOLANO: *A high order unfitted hybridizable discontinuous Galerkin method for linear elasticity*
- 2022-05 JAIME MANRÍQUEZ, NGOC-CUONG NGUYEN, MANUEL SOLANO: *A dissimilar non-matching HDG discretization for Stokes flows*
- 2022-06 RAIMUND BÜRGER, STEFAN DIEHL, MARÍA CARMEN MARTÍ, YOLANDA VÁSQUEZ: *A degenerating convection-diffusion system modelling froth flotation with drainage*

Para obtener copias de las Pre-Publicaciones, escribir o llamar a: DIRECTOR, CENTRO DE INVESTIGACIÓN EN INGENIERÍA MATEMÁTICA, UNIVERSIDAD DE CONCEPCIÓN, CASILLA 160-C, CONCEPCIÓN, CHILE, TEL.: 41-2661324, o bien, visitar la página web del centro: <http://www.ci2ma.udec.cl>



**CENTRO DE INVESTIGACIÓN EN
INGENIERÍA MATEMÁTICA (CI²MA)
Universidad de Concepción**



Casilla 160-C, Concepción, Chile
Tel.: 56-41-2661324/2661554/2661316
<http://www.ci2ma.udec.cl>

